Title

Integrated experimental and theoretical approach to probe the synergistic effect of ammonia in methanesulfonic acid reactions with small alkylamines

Journal

Environmental Science Processes & Impacts, 22(2)

ISSN

2050-7887

Authors

Perraud, Véronique
Xu, Jing
Gerber, R Benny
et al.

Publication Date

2020-02-26

DOI

10.1039/c9em00431a

Environmental Science Processes & Impacts

ROYAL SOCIETY OF CHEMISTRY

PAPER

View Article Online
View Journal | View Issue

Cite this: *Environ. Sci.: Processes Impacts*, 2020, **22**, 305

Integrated experimental and theoretical approach to probe the synergistic effect of ammonia in methanesulfonic acid reactions with small alkylamines†

Véronique Perraud, [a] Jing Xu, [b] R. Benny Gerber *[ac] and B. J. Finlayson-Pitts *[a]

Received 25th September 2019
Accepted 20th December 2019

DOI: 10.1039/c9em00431a

rsc.li/espi

While new particle formation events have been observed worldwide, our fundamental understanding of the precursors remains uncertain. It has been previously shown that small alkylamines and ammonia (NH_3) are key actors in sub-3 nm particle formation through reactions with acids such as sulfuric acid (H_2SO_4) and methanesulfonic acid ($CH_3S(O)(O)OH$, MSA), and that water also plays a role. Because NH_3 and amines co-exist in air, we carried out combined experimental and theoretical studies examining the influence of the addition of NH_3 on particle formation from the reactions of MSA with methylamine (MA) and trimethylamine (TMA). Experiments were performed in a 1 m flow reactor at 1 atm and 296 K. Measurements using an ultrafine condensation particle counter (CPC) and a scanning mobility particle sizer (SMPS) show that new particle formation was systematically enhanced upon simultaneous addition of NH_3 to the MSA + amine binary system, with the magnitude depending on the amine investigated. For the MSA + TMA reaction system, the addition of NH_3 at ppb concentrations produced a much greater effect (*i.e.* order of magnitude more particles) than the addition of ~12 000 ppm water (corresponding to ~45–50% relative humidity). The effect of NH_3 on the MSA + MA system, which is already very efficient in forming particles on its own, was present but modest. Calculations of energies, partial charges and structures of small cluster models of the multi-component particles likewise suggest synergistic effects due to NH_3 in the presence of MSA and amine. The local minimum structures and the interactions involved suggest mechanisms for this effect.

Environmental significance

Acid–base chemistry between gas phase precursors is recognized as an important source of new particles in air. Previous experimental and theoretical calculations have shown that small alkylamines play a critical role in sub-3 nm particles through reactions with strong acids such as sulfuric acid and methanesulfonic acid (MSA), the latter originating from oxidation of organosulfur compounds. As the energy landscape is transitioning away from fossil fuel sulfur dioxide, the MSA contribution to this chemistry is expected to be more important in the future. Alkylamines are ubiquitous in the atmosphere and they often co-exist with ammonia; thus synergism or competition between precursors may arise. This study highlights synergistic interactions between NH_3 and methylamine and trimethylamine in their reactions with MSA. Quantum calculations provide critical molecular insights into the central role that NH_3 plays in particle formation in these systems.

Introduction

New particle formation (NPF), the process by which gas phase precursors combine to give birth to particles in air, has been observed all around the world.[1–4] Such events have been measured in polluted urban areas,[5–7] above forest canopies,[8–11] in marine environments[12–14] and Arctic regions.[15,16] This phenomenon typically leads to the formation of stable molecular clusters that can further grow by uptake of trace gases and water to sizes sufficient to impact visibility,[17–19] public health[20–24] and climate.[25–28] Despite these observations, our understanding

[a]*Department of Chemistry, University of California, Irvine, CA 92697, USA. E-mail: bgerber@uci.edu; bjfinlay@uci.edu; Fax: +1-949-824-2420; Tel: +1-949-824-6758; +1-949-824-7670*

[b]*Department of Optical Engineering, Zhejiang A&F University, Lin'an 311300, Zhejiang, China*

[c]*Institute of Chemistry, The Fritz Haber Research Center, The Hebrew University of Jerusalem, Jerusalem 91904, Israel*

† Electronic supplementary information (ESI) available. See DOI: 10.1039/c9em00431a

of the mechanisms of nucleation and growth is still limited, with many open experimental and theoretical challenges.

There are many types of particles in air, and their properties vary greatly depending on the molecular constituents. An important type of airborne particle is that resulting from acid:base chemistry, with sulfuric acid reactions with ammonia and amines recognized as being particularly important in NPF.[29–54] Other species such as water[42,44,55–58] and organics[6,8,11,59–65] may also play a role in this chemistry. Acid:base systems involving HNO_3,[66–69] HCl[68,70,71] or small carboxylic acids[72–79] may contribute, although the interactions of the respective acids with ammonia and amines were found to be weaker than that with H_2SO_4.

Methanesulfonic acid ($CH_3S(O)(O)OH$, MSA), a strong acid ($pK_a = -1.9$),[80] is often formed alongside H_2SO_4 from the photooxidation of organosulfur compounds in air.[81] Previous experimental and computational studies from our laboratory have demonstrated that reaction of MSA with small alkylamines can be a significant source of NPF in air.[73,74,82–85] If emissions of sulfur dioxide (precursor to H_2SO_4 in air) associated with fossil fuel combustion continue to decline in the future as expected,[86–91] the relative contribution to NPF from MSA compared to H_2SO_4 will increase.[88] The concentration of gas phase MSA can be 10–100% of that of current H_2SO_4 concentrations,[92–99] and a role for MSA in particle formation is supported by field observations of MSA in smaller particles.[8,11,100–102]

Until now, most experimental and theoretical studies of acid:base particles have addressed particles made of one acid component (*e.g.* H_2SO_4 or MSA), and one base component (NH_3 or an amine), under dry or humid conditions. Enhancement of NPF due to small alkylamines was reported to be greater than that from NH_3 for both H_2SO_4 [29–33,37,41,48,52,54] and MSA reactions.[84] Additionally, amines have been observed to displace ammonia from clusters and particles for both acids.[67,103–106] A few studies investigated multi-component acid:base combinations with more than one acid.[73,74,107–110] However, studies investigating multi-component acid:base clusters and particles in which *both* an amine and NH_3 are present simultaneously at the onset of the nucleation have been reported thus far only for H_2SO_4.[31,32,52,111–114]

The present study adds to these recent findings with both experiments and quantum calculations for two specific MSA + amine + NH_3 systems, where the amines are a primary amine, methylamine (MA) and a tertiary amine, trimethylamine (TMA). These amines are both found in air along with NH_3.[115–118] The interactions in such systems are of fundamental and atmospheric interest. First, from a theoretical molecular point of view, one might expect proton transfer from the acid to the base to form a stable ion pair.[74,119–121] Previous studies combining proton transfer calculations and experiments on the same systems[74,119] suggest that proton transfer could be a good indicator for particle formation potential. For example, the MSA + MA system shows both proton transfer and high particle number concentrations, whereas, the MSA + NH_3 system exhibits no proton transfer under dry conditions, and is associated with little particle formation capacity. However, there are other factors to take into account as well, such as the possibility of forming hydrogen bond networks between the species. Indeed, while the MSA + TMA system exhibits a proton transfer between the acid and the base, this system is not experimentally efficient at forming particles due to the lack of a hydrogen bond network connecting the ion pairs. For reported multi-component H_2SO_4-based particles that include both an amine and NH_3, the issue of competition between the two potential acceptors of the proton then arises.[112–114] Related to this is the question of whether a *synergy* between NH_3 and the amine affects particle growth.[112,113] Under humid conditions, the issues are even more complex: does the presence of water molecules affect the efficiency of proton transfer or the synergism? How does it influence particle growth? These questions in such a complex system call for an integrated experimental and theoretical approach. This paper addresses these questions through experiments and calculations on multi-component MSA-based clusters, leading to insights into the location of the proton transfer and potential synergism between species with regards to particle formation.

This topic is also of significant relevance to NPF in the atmosphere. Gas phase amines and NH_3 are ubiquitous in air.[115] For example, they have been measured above oceans,[122,123] at urban[124–128] and agricultural sites,[116–118,129–132] from biomass burning,[117,133] and from vegetation and forested areas.[126,132,134–136] Ammonia almost always co-exists with amines and its gas phase concentration is typically an order of magnitude higher than that of the amines. Both ammonium and aminium ions have been frequently measured in the same particles that contain significant amounts of methanesulfonate.[8,11,16,100,137–141] This study is also of particular significance as NH_3 is ubiquitous in air both outdoors and indoors[132,142] due to its many sources, including human breath[143,144] and water or gas supplies used in laboratory studies.[7,29,33,34,45,53,111,145,146]

Experimental methods

(1) Flow reactor description

Formation of detectable (>2.0 nm) nanoparticles was investigated using two 1-m borosilicate flow reactors over reaction times from 0.3 to 6 s at 296 K and 1 atm (Fig. 1). The characteristics of the flow reactors have been described elsewhere[73,74,83–85,147] and details for both configurations are presented in the ESI.† Briefly, both reactors had fixed ring inlets at the upstream end of the reactor and spoked inlets mounted at the end of a set of movable concentric tubes. One reactor had three fixed ring inlets (rings A–C) located at the upstream end of the flow reactor and three spoked inlets (spokes 1–3) while the second had two fixed rings (rings A and B) and two movable spoked inlets (spokes 2 and 3). A total of ~17 L min^{-1} of dry clean air flowed through the reactor and was distributed as follows: 13 L min^{-1} was introduced at ring A, 1 L min^{-1} (mixed with NH_3) was either introduced at ring B or spoke 1, with 2 L min^{-1} at spoke 2 (MSA injection port) and 1 L min^{-1} at spoke 3 (MA or TMA injection port). The flow reactor temperature was maintained at 296 K using a water jacket. Prior to each set of experiments, the flow reactor was cleaned with nanopure water and dried with dry clean air with the water jacket set at 343 K.

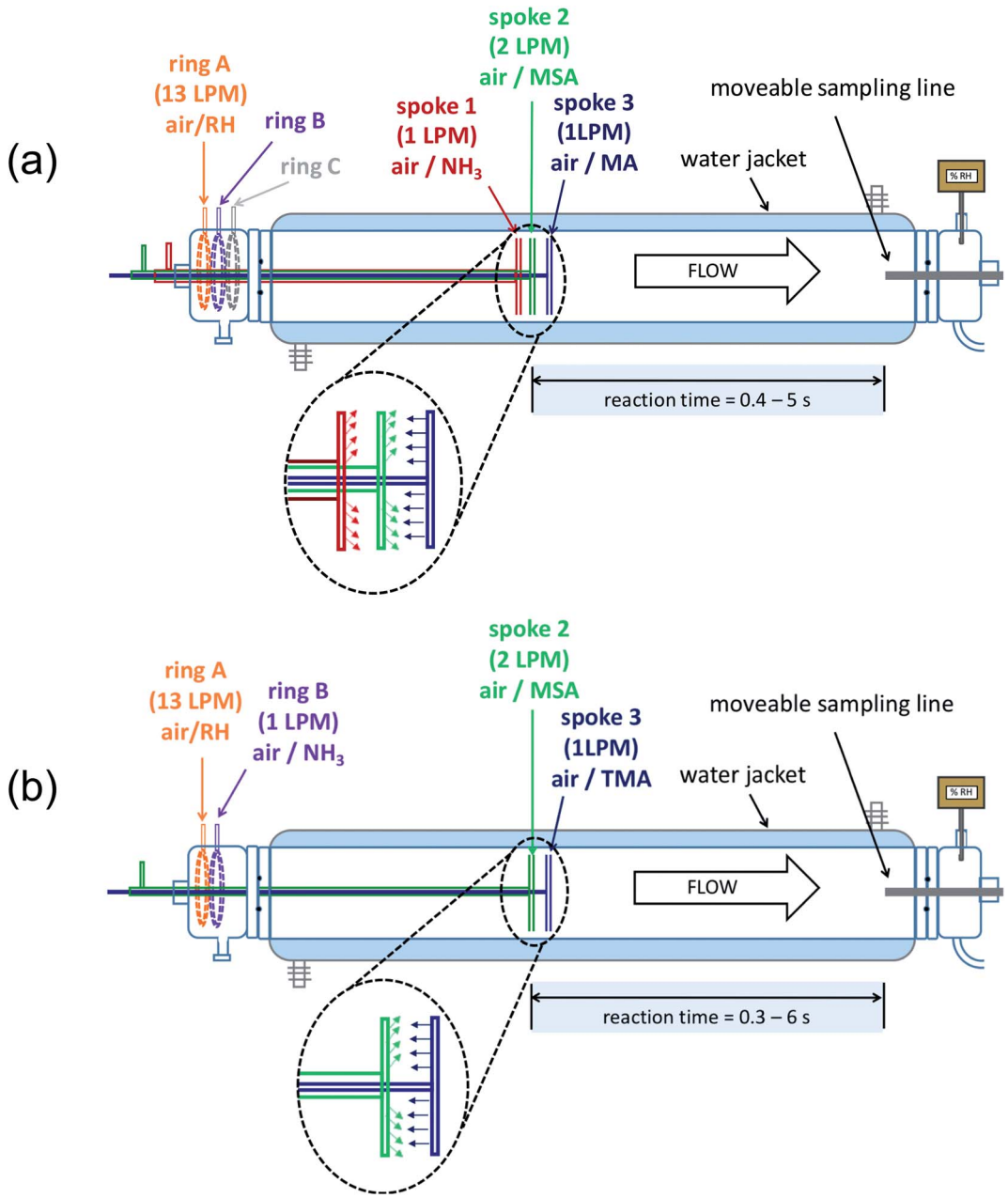

Fig. 1 Schematics of the flow reactors used to investigate new particle formation from (a) the MSA + MA (± NH_3) reaction and (b) the MSA + TMA (± NH_3) reaction. The diagrams are adapted from ref. 73 and 147.

The flow reactor was conditioned with a flow of gas phase MSA for at least two days prior to experiments.

These studies were performed using dry clean air provided by a purge air generator (Parker-Balston, model 75-62) followed by a purification system composed of carbon/alumina media (Perma Pure, LLC) and a 0.1 μm filter (DIF-N70; Headline Filters). To minimize contaminant NH_3 that might be present in purge air, in most experiments the entire 13 L min^{-1} of the air feeding the first ring inlet (ring A) was passed through a trap containing phosphoric acid (H_3PO_4; ACS grade, EMD) coated glass beads followed by a drierite drying trap (anhydrous calcium sulfate, 100%; W. A. Hammond Drierite Company LTD) prior to being added to the flow tube. Note that it was not experimentally possible for the entire flow of purge air to be treated, but the 13 L min^{-1} represents 76% of the total air flow. Blank measurements of air flowing through the reactor were performed by collecting air in custom-made cartridges containing 150 mg of glass wool as the sorbent material. The cartridges were extracted successively three times with 10 mL of 0.05 M oxalic acid aqueous solution followed by ion chromatography analysis (Dionex ICS 1100). The solution was freshly made each day from pure oxalic acid (Aldrich, 98%). No measurable NH_3 was found, suggesting that if a small amount

of NH_3 was present, it was lower than the 10 ppt limit of detection.

In each experiment, the reaction of MSA with MA or TMA took place at the spoked inlets, while NH_3 was added either at one of the upstream rings or at the upstream spoke (spoke 1; Fig. 1a). In either case, all reactants were present simultaneously rather than reacting sequentially. Variable relative humidity (RH) inside the flow reactor was achieved by diverting part of the 13 L min^{-1} flow of air (ring A) through a bubbler filled with Nanopure™ water (18.2 MΩ cm; model 7146; Thermo Scientific, Barnstead) to yield RH < 3% to ~45–50% (corresponding to a water vapor concentration of $\sim 3 \times 10^{17}$ molecules per cm^3 at $T = 296$ K). The RH was monitored with an RH probe (model HMT338; Vaisala) located in the end cap of the flow reactor. The nanopure water was analyzed using the IC system described above to verify that it did not contain any NH_3 contamination, and the water trap was refilled with fresh water prior to each experiment. Particles were sampled through a moveable 0.635 cm o.d. stainless steel tube mounted on the downstream end-cap of the flow tube to access reaction times ranging from 0.4 s to 5.3 s (MSA + MA system) and 0.3 s to 5.9 s (MSA + TMA system). Total particle number concentrations and size distributions were measured as a function of reaction time as described below.

(2) Reactants

Gas phase MSA was generated by passing 0.1 or 0.2 L min^{-1} of dry clean air over the pure liquid (Sigma-Aldrich, ≥99%) which was maintained at room temperature in a glass trap. Periodically, the entire flow of MSA was directed into a 0.45 μm Durapore filter (Millex-HV) for 10 min. After sampling, the filter was extracted with 10 mL of nanopure water (each filter was extracted with 3 × 3 mL of nanopure water flow in the opposite direction to that used for sampling. This was followed by one additional extraction with 1 mL of nanopure water and the extracts were combined together to yield a 10 mL sample). The combined extracts were then analyzed by UPLC-ESI-MS/MS (Quattro Premier XE, Waters; MRM method following the m/z 95 ⇒ m/z 80 transition). Note that during the development of the method, a second extraction of the filter was performed and the second extract did not show any traces of MSA, suggesting that one extraction is efficient at extracting all of the MSA collected. In some occasions, collection of the MSA exiting the trap was performed with two filters in series, but no MSA was measured in the second filter. Each measurement was done in triplicate.

Gas phase MA and TMA were generated by flowing dry clean purge air over commercially available permeation tubes containing the amines (VICI Metronics) that were maintained in a U-shaped glass trap at room temperature. The concentration of amine exiting the traps was determined periodically by ion chromatography (Dionex ICS 1100) after trapping the gases onto a custom-made cation-exchange resin, followed by three successive extractions with 10 mL of a 0.05 M oxalic acid aqueous solution flow in the opposite direction to that used for sampling.[116] The sum of the these three extractions was used for quantification, and each permeation tube measurement was done in triplicate. No quantifiable ammonia or other contaminants were detected for either permeation tube. The concentrations of the reactants determined herein may be upper limits due to potential wall losses even after extensive conditioning.

(3) Particle measurements

Total particle number concentrations (N_{total}, particles per cm^3) were measured at each reaction time using an ultrafine butanol-based condensation particle counter (CPC; model 3776; TSI; flow rate 1.5 L min^{-1}). Detectable particles are defined hereafter as those with a mobility diameter greater than 2.0 nm, which is the lowest diameter size the 3776 CPC can measure. The counting efficiency increases from 0% at 2.0 nm to 100% at 3.0 nm with a manufacturer-specified d_{50} for this instrument of 2.5 nm defined as the diameter at which 50% of the particles are detected based on sucrose particles. Note that due to this limitation, the initial clusters nucleated from the present reactions were not detected, and it is only those that have grown to diameters > 2.0 nm that were measured; thus our measurements include nucleation and the first steps of growth. Parallel measurements using a combination of the CPC with a particle size magnifier (PSM; model A10; Airmodus)[148] leading to a lower diameter cut-off were also performed. As described in the ESI,† the operating conditions were set so that the d_{10}, d_{50} and d_{80} cut-offs (diameters at which 10%, 50%, and 80% of the particles are detected respectively) were 1.2 nm, 1.4 nm and 2.1 nm respectively, according to the manufacturer calibration using negatively charged ammonium sulfate particles. It is recognized that the true cut-off sizes for both the CPC and PSM strongly depends on the chemical composition of the particle sampled.[148–153] The cut-off sizes for the present MSA + amine particles are not known, thus the cut-offs defined for the reference compounds are applied here. Despite these distinctions, as reported in Fig. S1 and S2† no significant differences were observed between the CPC and the combination PSM + CPC measurements for any of the systems studied. Thus, N_{total} values are reported hereafter for the CPC and SMPS as described below. Measurements with a HEPA filter at the beginning of each experiment were performed to ensure there was a zero background reading. When necessary (*i.e.* total counts > 3×10^5 particles per cm^3), the particle stream exiting the flow tube was diluted with purge air prior to entering the CPC.

Particle size distributions were also measured using a scanning mobility particle sizer (SMPS; TSI) equipped with a 0.071 cm impactor nozzle, a ^{210}Po bipolar charger (10 mCi; model 2021; NRD), an electrostatic classifier (model 3080; TSI), a nano differential mobility analyzer (nanoDMA; model 3085; TSI) and the 3776 model CPC. The SMPS was operated with the following settings: sheath air flow rate, 15 L min^{-1} (recirculating mode); sample flow rate, 1.5 L min^{-1}. Under these conditions, the SMPS measured particles with mobility diameters ranging from 2 nm to 64 nm. To test for changes in the size distributions due to drying within the SMPS, some TMA experiments were carried out in which the sheath air was humidified to an RH of ~52% (apparatus shown in Fig. S3a†). The MSA + TMA combination was chosen because it is the most hygroscopic of the two systems studied and is thus expected to

be most sensitive to water.[154,155] As shown in Fig. S3b,† the size distributions were very similar between measurements performed with humid sheath air (RH ~ 52%) *versus* those performed with dry recirculating air. No significant changes in the mobility geometric mean diameter (GMD) were observed when the sheath air was externally humidified (difference of only 2.9%). However, there was an apparent loss of the smallest particles with diameter < 20 nm (13% lower total number concentration for the humid runs compared to the dry recirculating sheath air runs). The use of an external dry air supply (Fig. S3c†) produced a slightly stronger drying effect (difference in GMD of 4.1%). For simplicity, all measurements were carried out with dry recirculating sheath air (*i.e.* normal SMPS operating conditions) where the loss of the smallest particles is minimized. To avoid potential reaction time bias, all particle measurements were performed after the system had reach steady state in the following order: 5.3–5.9 s, 2.9–3.1 s, 0.28–0.37 s, 1.6–1.7 s, 4.2–4.5 s and 5.3–5.9 s (the range represents the times for the two different flow tubes). Data collected from the SMPS were also used to estimate particle formation rates ($J_{>2.0\mathrm{nm}}$) following the linear change in total particle number concentration (N_{total}) as:[2]

$$J_{>2.0\mathrm{nm}} = \frac{\Delta N_{\mathrm{total}}}{\Delta_t} \quad (1)$$

The determined $J_{>2.0\mathrm{nm}}$ values represent apparent particle formation rates for each condition, as this treatment does not separate out processes such as the real nucleation rate of the smallest clusters (too small to see using our instrumentation), coagulation, scavenging or wall losses of the particles throughout the flow reactor (those processes might be more important at the largest concentrations observed, *i.e.* $>10^7$ particles per cm^3).

Theoretical methods

In this study, quantum calculations were carried out for small clusters of the precursor gases to provide theoretical insights into the formation and growth of particles in the MSA + amine ($\pm$ NH_3) ($\pm$ H_2O) systems. Thus, calculations of the energies, structures and partial charge distributions of relevant multi-component clusters were calculated using density functional methods. The effectiveness of this approach was previously demonstrated for clusters that include binary MSA–amine clusters and ternary MSA–amine–H_2O clusters.[74,82,85,119–121,154,156,157] Similar approaches were previously used for acid:base particles containing H_2SO_4 with an amine or NH_3, and water.[30,54,55,157–160]

Proton transfer to the amine was generally found for the lowest energy clusters, and this seems a key feature consistent with the interpretation of experimental observations.[119] One must therefore employ quantum-chemical potentials that can adequately describe the acid + amine reaction, in addition to the hydrogen-bonding and Van der Waals interactions that are involved. The presence of both an amine and NH_3 in the multi-component clusters implies that competition for the MSA proton may take place. Accurate treatment of the proton transfer is thus essential.

All of the electronic structure calculations including geometry, frequency, and energy calculations were done using B3LYP variant[161–163] of density functional theory (DFT) with Grimme's dispersion correction.[164] The Dunning augmented double-ζ correlation-consistent basis set was employed. Note that basis set superposition errors were not considered here, based on the fact that the contribution of this effect was previously tested for similar systems,[165] and found to be small. In previous studies,[119] this method was tested against the MP2 method and the high level CCSD(T) method for the low-lying isomers of the binary MSA–MA cluster. The results show better-than-qualitative agreement between the three methods and support the adequacy of the B3LYP-D3 method for our purpose. There is evidence that DFT variants with hybrid functionals (including B3LYP) with Grimme's dispersion interaction corrections are reasonably successful methods in predicting the global minimum structures of hydrogen-bonded clusters and the structures of low-lying conformers of involved water molecules.[166–169] Hence, B3LYP-D3 was chosen here as it offers a reasonable level of accuracy while being computationally efficient.

The initial structures of each system were randomly generated in an 8 × 8 × 8 Å cube with a minimum distance criterion of 1.8 Å between each molecule using the PACKMOL package.[170,171] Using this program, 300 different initial structures were generated for each system, and energy minimization was carried out for these structures. To obtain Gibbs free energies (ΔG), the contribution from vibrational entropy was computed for each structure (at 298 K) and added in. Dissociation energies (D_e) and Gibbs free energies (ΔG) are calculated as followed: $D_e = E(\mathrm{AB}) - E(\mathrm{A}) - E(\mathrm{B})$ and $\Delta G = G(\mathrm{AB}) - G(\mathrm{A}) - G(\mathrm{B})$. Note that the aug-cc-pVDZ basis may not always be sufficiently accurate for binding energies, but most often that basis set is adequate, and this is likely to be the case also here. All of the structures reported here were geometrically optimized at the level of B3LYP-D3/aug-cc-pVDZ. Note that no imaginary vibrational frequencies were observed in any of the cases presented, and all cases have the correct number of positive frequencies. In addition, zero-point energies (ZPE) were used to correct electronic energy values. Partial charges (denoted by δ) were calculated using natural bond orbital (NBO) analysis.[172,173] All the calculations presented in this paper were performed using the Q-CHEM 4.3 program package.[174]

Results and discussions

(A) MSA + MA ($\pm$ NH_3) reaction

(1) Dry conditions. Fig. 2a shows the total number concentrations of particles (N_{total}) measured using the CPC for the MSA + MA system ([MSA] = 6.4×10^{10} molecules per cm^3; [MA] = 6.1×10^{10} molecules per cm^3), with or without NH_3 as a function of reaction time. In the absence of NH_3, nucleation of new particles is already extremely efficient with N_{total} ranging from ~50 particles per cm^3 at 0.37 s to $(7.4 \pm 1.1) \times 10^4$ particles per cm^3 at 5.3 s. Upon the addition of NH_3 (2.9×10^{11} molecules per

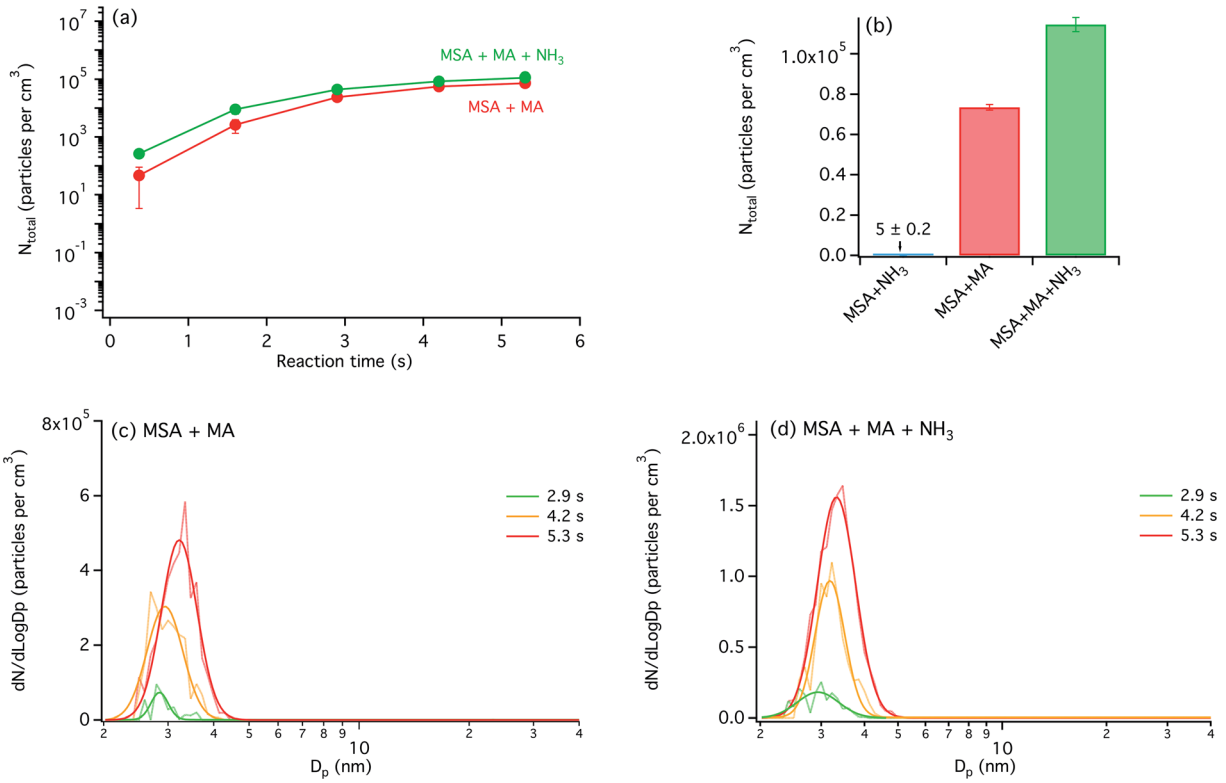

Fig. 2 (a) Total particle number concentrations (N_{total}) from MSA + MA and MSA + MA + NH_3 reactions as a function of reaction time measured using the CPC (dry conditions). Each data point corresponds to the average N_{total} measured over a 5 min scan (error bars correspond to 1 standard deviation). (b) Comparison of N_{total} values measured at 5.3 s for MSA + NH_3, MSA + MA and MSA + MA + NH_3 reactions. Size distributions measured using the SMPS are presented in (c) for the MSA + MA and (d) for the MSA + MA + NH_3 reactions respectively. Each size distribution is given in light colors with a log normal fit to guide the eye (each distribution corresponds to an average from five successive scans, except for reaction time 5.3 s where ten scans were averaged instead (standard deviation are not shown for clarity)). Concentrations of reactants for all panels are [MSA] = 6.4×10^{10} molecules per cm^3; [MA] = 0 or 6.1×10^{10} molecules per cm^3; [NH_3] = 0 or 2.9×10^{11} molecules per cm^3.

cm^3) to the MSA + MA system, the same trend is observed as a function of reaction time, with N_{total} being systematically higher than that measured in the absence of NH_3. An enhancement factor (EF), defined as N_{total} measured at 5.3 s in the presence of NH_3 (or H_2O) ratioed to that measured in the absence of NH_3 (or H_2O) was determined from this CPC dataset. The EF observed for MSA + MA (± NH_3) is modest, with a value of 1.6 ± 0.1 (Table 1). A separate series of measurements was performed under which MSA was in excess compared to MA ([MSA]/[MA] ~ 2; [MSA] = 4.6×10^{10} molecules per cm^3; [MA] = 2.3×10^{10} molecules per cm^3), and again a modest enhancement was observed when NH_3 (1.1×10^{11} molecules per cm^3) was added to the flow reactor (average factor of 1.7 ± 0.8; Fig. S4†). These enhancements may be lower limits as particles

Table 1 Total particle number concentration enhancement factors (EF) for each MSA + amine reaction[a]

Reference case	[MSA] (molecules per cm^3)	[H_2O] (molecules per cm^3)	Enhancement factor (EF_{CPC}) +H_2O[b]	Enhancement factor (EF_{CPC}) +NH_3	Enhancement factor (EF_{SMPS}) +H_2O[b]	Enhancement factor (EF_{SMPS}) +NH_3
Methylamine ([MA] = 6.1×10^{10} molecules per cm^3)						
MSA + MA	6.4×10^{10}	—	63 ± 1.3	1.6 ± 0.1[c]	$(2.0 \pm 0.4) \times 10^2$	3.7 ± 0.7[c]
MSA + MA + H_2O	6.4×10^{10}	~3×10^{17}	—	1.1 ± 0.02[c]	—	0.86 ± 0.1[c]
Trimethylamine ([TMA] = 5.0×10^{10} molecules per cm^3)						
MSA + TMA	7.9×10^{10}	—	$(1.8 \pm 0.4) \times 10^2$	$(1.1 \pm 0.3) \times 10^4$ [d,e]	n/a[f]	n/a[f]
MSA + TMA + H_2O	7.9×10^{10}	~3×10^{17}	—	$(2.6 \pm 0.5) \times 10^2$[d]	—	$(3.8 \pm 0.7) \times 10^2$[d]

[a] From data in Fig. 1 and 2 (MA) and Fig. 5 and 7 (TMA). [b] Experiments performed at ~45–50% RH corresponding to ~3×10^{17} molecules per cm^3. [c] [NH_3] = 2.9×10^{11} molecules per cm^3. [d] [NH_3] = 2.2×10^{10} molecules per cm^3. [e] Enhancement factors up to 1.1×10^6 were observed for [NH_3] = 1.0×10^{11} molecules per cm^3 (see Fig. 5; [MSA] = 6.4×10^{10} molecules per cm^3; [TMA] = 4.8×10^{10} molecules per cm^3). [f] The MSA + TMA reaction did not generate enough particles to be observable by the SMPS.

formed from the MSA + MA + NH_3 condition were approaching the limit for efficient CPC counting. Fig. 2b presents the comparison between the mixed MSA + MA + NH_3 system and the respective MSA + MA and MSA + NH_3 systems ([MSA] = 6.4 × 10^{10} molecules per cm^3; [MA] = 0 or 6.1 × 10^{10} molecules per cm^3; [NH_3] = 0 or 2.9 × 10^{11} molecules per cm^3). It is evident that a modest synergy is present for this system, and the effect is simply not just additive: the MSA + NH_3 system is not efficient at forming particle on its own (only 5 particles per cm^3 were observed at 5.3 s, despite the large concentration of NH_3); however, the addition of NH_3 to the MSA + MA system enhances the total number of detectable particles by a factor of 2 compared to the MSA + MA binary system, as described above. It is likely that NH_3 grew the initial MSA + MA clusters that were too small to be detected to now be within the measurable range of our instrumentation (>2 nm). These results thus show the first evidence for a synergism between MA and NH_3 in forming particles with MSA.

Experiments for which reaction time (5.3 s) and initial MSA concentration ([MSA] = 6.4 × 10^{10} molecules per cm^3) were fixed are illustrated in Fig. S5.† Fig. S5a† (filled red squares; no NH_3) shows that N_{total} is correlated with the MA concentration, with few particles (<40 particles per cm^3) observed for MA concentrations smaller than 1.7 × 10^{10} molecules per cm^3 (excess MSA conditions). For MA concentrations larger than 3.2 × 10^{10} molecules per cm^3, a significant particle number concentration is observed (>5000 particles per cm^3). Previous studies[154,156] predicted that MA can form tight nanosize $(MSA–MA)_4$ clusters with MSA that are extremely stable due to a substantial hydrogen bonding network, consistent with these observations. Indeed, quantum calculations indicated that the dissociation energies (D_e at 0 K as well as ΔG at 298 K) of this cluster into various smaller complexes were endothermic. In addition, dynamics showed that this cluster was stable for at least 100 ps at temperatures up to 500 K, well above atmospheric temperatures. Note that, on the other hand, the MSA + NH_3 system (Fig. 2b and S5b;† filled red triangles) itself is not as efficient at forming particles, with N_{total} only reaching ~5 particles per cm^3 for NH_3 concentration of 2.9 × 10^{11} molecules per cm^3 under dry conditions at 5.3 s.

Fig. 2c and d show the size distributions for MSA + MA and MSA + MA + NH_3 conditions. Small particles with mobility diameters < 5 nm were observed for the MSA + MA system ([MSA] = 6.4 × 10^{10} molecules per cm^3; [MA] = 6.1 × 10^{10} molecules per cm^3), and in presence of NH_3 (2.9 × 10^{11} molecules per cm^3), N_{total} increased but no significant growth was observed. The mobility geometric mean diameter (GMD) for particles measured at 5.3 s without NH_3 was 3.2 ± 0.1 nm, while it was 3.3 ± 0.1 nm in presence of NH_3 (Fig. S6a†). In brief, NH_3 has only a modest impact on the MSA + MA system under dry conditions. Based on the SMPS data collected as a function of reaction time, particle formation rates ($J_{>2.0nm}$) were determined (Fig. S6b†). The

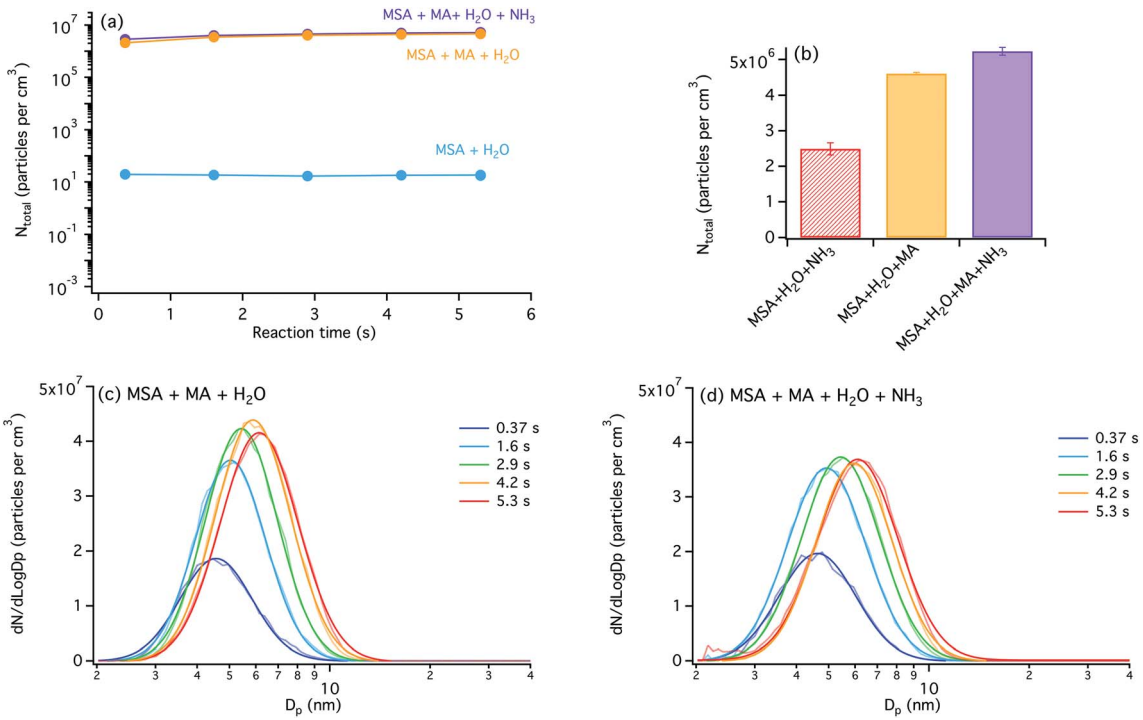

Fig. 3 (a) Total particle number concentrations (N_{total}) from MSA + H_2O, MSA + MA + H_2O and MSA + MA + H_2O + NH_3 reactions as a function of reaction time measured using the CPC (RH ~ 45–50%). Each data point corresponds to the average N_{total} measured over a 5 min scan (error bars correspond to 1 standard deviation). (b) Comparison of N_{total} values measured at 5.3 s for MSA + H_2O + NH_3, MSA + H_2O + MA and MSA + H_2O + MA + NH_3 reactions. Size distributions measured using the SMPS are presented in (c) for the MSA + MA + H_2O and (d) for the MSA + MA + H_2O + NH_3 reactions respectively. Each size distribution is given in light colors with a log normal fit to guide the eye (each distribution corresponds to an average from five successive scans, except for reaction time 5.3 s where ten scans were averaged instead (the standard deviation is not shown for clarity)). Concentrations of reactants for all panels are [MSA] = 6.4 × 10^{10} molecules per cm^3; [MA] = 0 or 6.1 × 10^{10} molecules per cm^3; [NH_3] = 0 or 2.9 × 10^{11} molecules per cm^3.

resulting values of $J_{>2.0nm}$ for MSA + MA and MSA + MA + NH_3 systems are $(2.2 \pm 0.4) \times 10^4$ particles per cm^3 per s and $(8.0 \pm 0.7) \times 10^4$ particles per cm^3 per s respectively.

(2) In the presence of water vapor. Fig. 3a shows N_{total} values measured using the CPC for the MSA + MA + H_2O system at ~45–50% RH with and without NH_3 as a function of reaction time ([MSA] = 6.4×10^{10} molecules per cm^3; [MA] = 6.1×10^{10} molecules per cm^3). Comparing Fig. 2a (MSA + MA; red trace) and Fig. 3a (MSA + MA + H_2O; orange trace), it is apparent that the addition of water vapor alone (without added NH_3) increases the total number of particles detected, leading to N_{total} values of ~10^7 particles per cm^3 at 5.3 s (enhancement factor of 63 ± 1.3 compared to the dry case; Table 1). The size distribution with water present (Fig. 3c) showed larger particles than the corresponding dry system with GMD of 4.7 ± 0.07 nm at 0.37 s and 6.1 ± 0.1 nm at 5.3 s (Fig. S7†), compared to ~3 nm for the dry system. This is consistent with a previous study[154] where a large enhancement in particle formation and growth was observed for MSA + MA when water was added *simultaneously with* MSA and MA (measurements performed at $t = 13.9$ s). In contrast, *subsequently* exposing initially dry particles from MSA + MA reaction to water vapor did not enhance particle formation or significantly grow them (in this case, the MSA and MA reacted for 8.2 s before interacting with water vapor for an additional 5.7 s to reach the sampling line). A proposed molecular explanation based on quantum chemical calculations[154] is that in the former case, water molecules incorporated into the cluster can act as the hydrogen bond donor and acceptor for the initial cluster to grow, whereas in the latter case, the tight MSA–MA ion pair system is too stable to be disrupted by water molecules. By comparison, MSA + H_2O itself only formed about 20 particles per cm^3 throughout the flow reactor at ~45–50% RH (light blue trace in Fig. 3a). Fig. S5a† shows near identical N_{total} values for the MSA + MA + H_2O reaction at both ~18% RH and 45–50% RH.

In the presence of NH_3 (Fig. 3a; [NH_3] = 2.9×10^{11} molecules per cm^3) no apparent enhancement is observed. As seen in Fig. 3c, d and S7a,† the particles did not grow upon addition of NH_3, and N_{total} is similar at 5.3 s (Fig. S7b†). Either with or without NH_3, a plateau in the number concentrations is observed after 1.6 s, suggesting that particles form quickly (0–1.6 s) and then continue to slowly grow by condensation of vapors. This highlights the role of water in the growth of particles when present as MSA and MA are reacting, consistent with our earlier studies.[73,85,154]

It is noteworthy that the MSA + NH_3 + H_2O reaction where [NH_3] = 2.9×10^{11} molecules per cm^3 (with [MSA] = 6.4×10^{10} molecules per cm^3) actually produces a similar number of particles to the MSA + MA + H_2O reaction (Fig. S5;† [MSA] = 6.4×10^{10} molecules per cm^3; [MA] = 6.1×10^{10} molecules per cm^3). The effect of NH_3 (2.8×10^{11} molecules per cm^3) on the MSA + MA + H_2O system is not additive (Fig. 3b and S8†), and little enhancement in N_{total} is observed. This suggests that most of the MSA is tied up with MA and water, and little is left in its 'free' form to interact with NH_3. It also suggests that NH_3 does not disrupt the MSA–MA–H_2O clusters. Chemical composition measurements on these sub-20 nm particles would confirm the presence or absence of NH_3 in these particles, but was outside of the scope of this paper.

From the SMPS data collected as a function of time (Fig. 3c and d), particle formation rates ($J_{>2.0nm}$) were estimated to be 1.4×10^7 particles per cm^3 per s (no NH_3) and 1.5×10^7 particles per cm^3 per s (with NH_3) (Fig. S7b†), which are much higher than the dry case, highlighting the importance of water in this system.

(3) Insights from theoretical calculations. The structures of the most stable MSA–MA clusters with and without NH_3 are shown in Fig. 4. The corresponding energies for dissociation to the monomers, and corresponding Gibbs free energies are listed in Table 2. First, for the 1MSA–1MA (Fig. 4a) and 2MSA–2MA (Fig. 4c) clusters without NH_3, the most stable structures involve a proton transfer (δ = 0.83–0.85) from the acid to the base forming an ion pair, consistent with our previous studies.[85,119]

For the 1MSA–1MA–1NH_3 (Fig. 4b) and 2MSA–2MA–2NH_3 (Fig. 4d) clusters, the key skeletons of the clusters do not change significantly compared to those without NH_3, and the positive charges on NH_3 (δ = 0.06) mean that NH_3 makes only a small contribution to charge transfer from MSA. Note that extensive sampling of the initial configurations was carried out using the PACKMOL code. In principle, this approach should reveal significant changes in structural parameters, if such changes indeed occur. The dominant charge acceptor (δ = 0.79–0.81) remains the stronger base, MA (gas phase basicity, GB, is 864.5 kJ mol^{-1} for MA *versus* 819.0 kJ mol^{-1} for NH_3).[175] When compared to those without NH_3, the dissociation energies of clusters with NH_3 increase from 15 to 29 kcal mol^{-1} for the 1MSA–1MA–1NH_3 cluster and from 68 to 92 kcal mol^{-1} for the 2MSA–2MA–2NH_3 cluster (Table 2). The corresponding Gibbs free energies increase from 4 to 10 kcal mol^{-1}, and from 35 to 40 kcal mol^{-1}, respectively. The fact that the energies are systematically higher in the presence of NH_3 indicates that the species are more strongly bound to each other within the cluster and that the cluster, if formed, is more thermodynamically stable with respect to dissociation compared to that without NH_3. In brief, the main effect of NH_3 in the MSA + MA system is to provide hydrogen bonds to MSA and MA, forming a more stable closed structure. Furthermore, although the skeletons of clusters with and without NH_3 do not change significantly, the addition of NH_3 provides extra hydrogen bond opportunities to incoming gas phase molecules where they can potentially attach to grow the initial clusters to detectable particles. These calculations are consistent with the experimental findings where only a modest enhancement in particle number concentration was observed upon addition of NH_3.

The structures of the 1MSA–1MA–1H_2O and 2MSA–2MA–2H_2O clusters with and without NH_3 are shown in Fig. 4e–h, and the corresponding dissociation energies and Gibbs free energies are given in Table 2. In all these clusters, the proton is always transferred from MSA to MA whether or not NH_3 is present, similar to the dry conditions. For comparison, Wang *et al.*[114] recently reported quantum calculations in which all the 1H_2SO_4–1MA–1NH_3 clusters investigated with various numbers of water molecules systematically show proton transfer from the acid to MA. For the MSA + MA system presented here, the role of

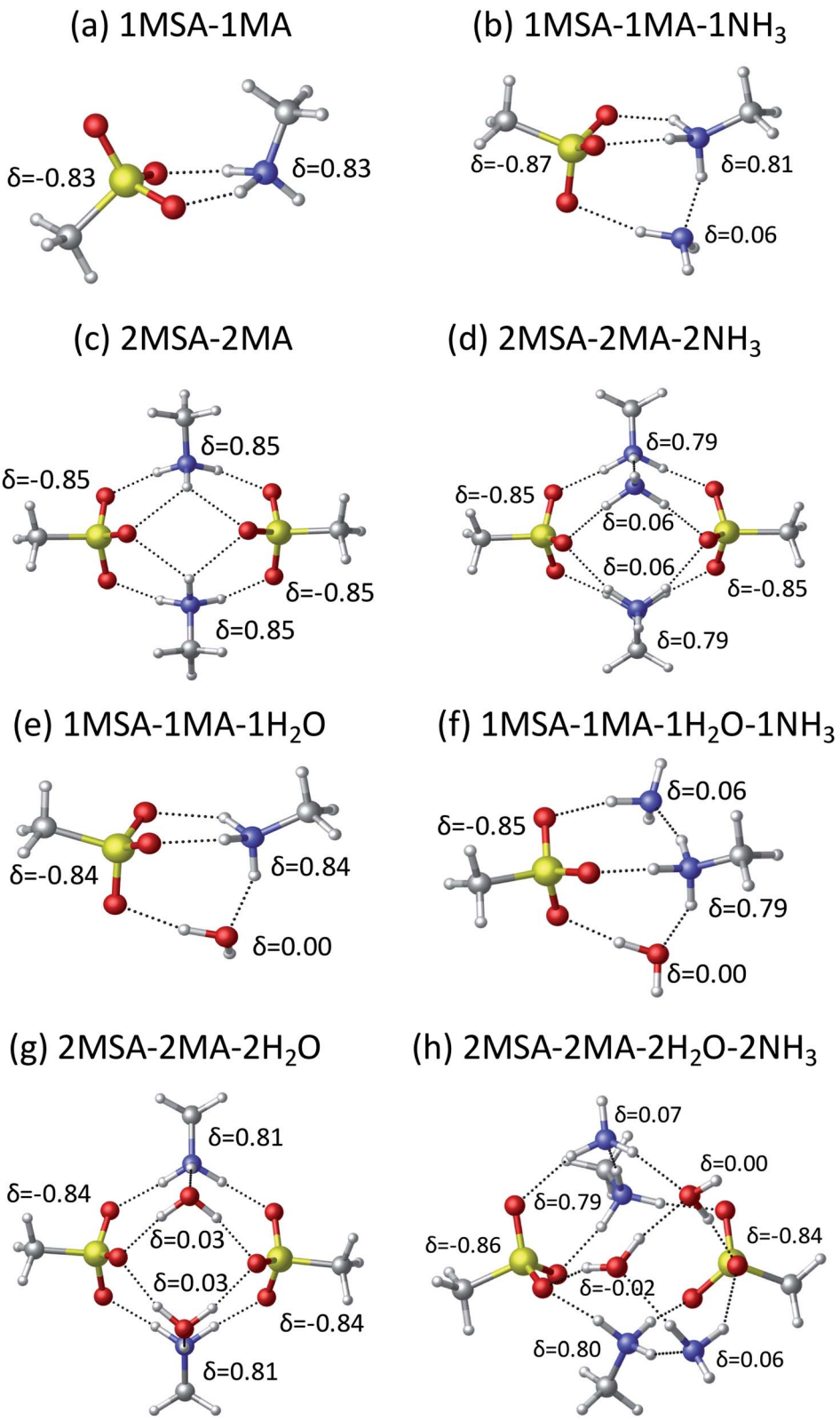

Fig. 4 Structures with distances (in angstroms) and partial charges δ (in atomic units) of the most stable structures of complexes composed of MSA, MA, NH_3 and H_2O at the level of B3LYP-D3/aug-cc-pVDZ. Structures (a) and (c), (b) and (d), (e) and (g), (f) and (h) are the mono-cluster and dimer cluster of MSA–MA, MSA–MA–NH_3, MSA–MA–H_2O, MSA–MA–H_2O–NH_3 respectively.

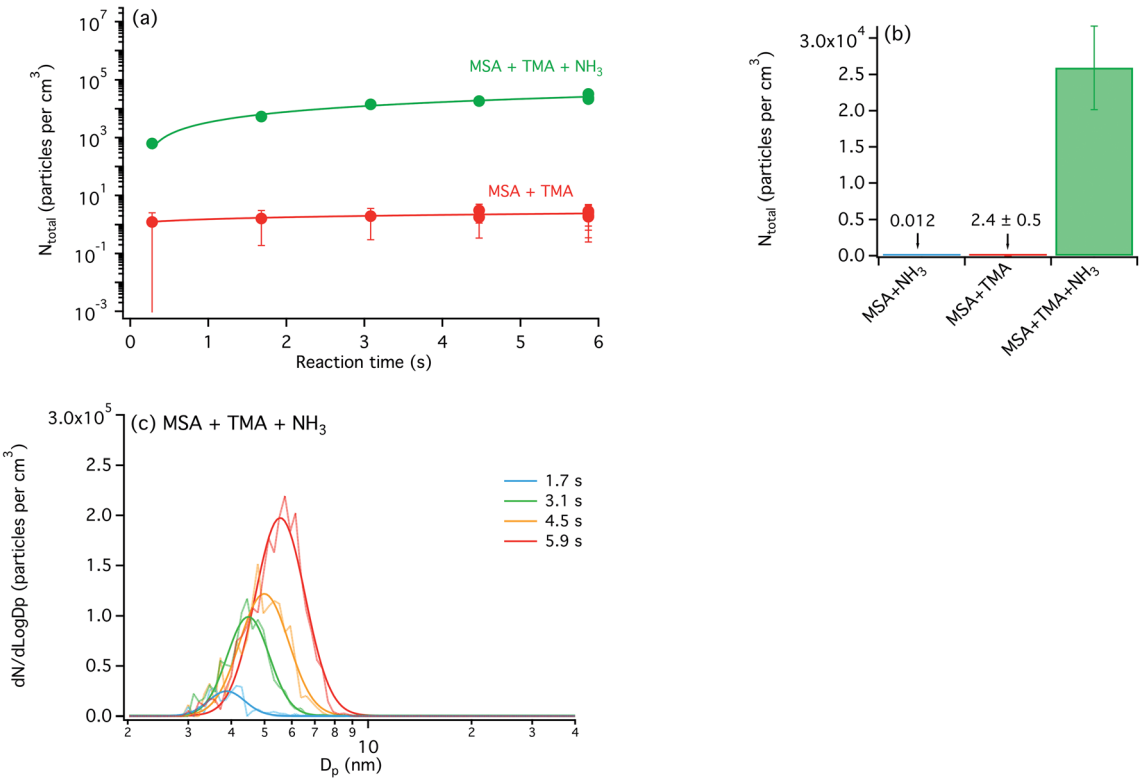

Fig. 5 (a) Total particle number concentrations (N_{total}) from MSA + TMA and MSA + TMA + NH_3 reaction systems as a function of reaction time measured using the CPC (dry conditions). Each data point corresponds to the average N_{total} measured over a 5 min scan (error bars correspond to 1 standard deviation). (b) Comparison of N_{total} values measured at 5.9 s for MSA + NH_3, MSA + TMA and MSA + TMA + NH_3 reactions. (c) Size distribution for the MSA + TMA + NH_3 reaction (the MSA + TMA reaction didn't generate enough particles to be observable by the SMPS). Each size distribution is given in light colors with a log normal fit to guide the eye (each distribution corresponds to an average from five successive scans, except for reaction time 5.9 s where ten scans were averaged (standard deviation are not shown for clarity)). Concentrations of reactants for all panels are [MSA] = 7.9×10^{10} molecules per cm^3; [TMA] = 0 or 5.0×10^{10} molecules per cm^3; [NH_3] = 0 or 2.2×10^{10} molecules per cm^3. Note that at 0.28 s, particles (>2.0 nm) were not detectable using the SMPS for the MSA + TMA + NH_3 reaction.

NH_3 is analogous to that of H_2O, as both can form more hydrogen bonds within the clusters, stabilizing their structures compared to that of the corresponding MSA + MA system (Table 2). Both also have the capability of hydrogen bonding to incoming molecules. For example, the 1MSA–1MA–1H_2O (Fig. 4e) exhibits one free –OH on the water molecule, while the 2MSA–2MA–2H_2O (Fig. 4g) exhibits two hydrogen bond acceptor sites on the water oxygens. Similarly, for the 1MSA–1MA–1NH_3 cluster (Fig. 4b), the cluster has two potential hydrogen bond donor sites located on the NH_3, while for the 2MSA–2MA–2NH_3 cluster (Fig. 4d) there is one on each ammonia. From the viewpoint of partial charge, NH_3 has only a small contribution ($\delta = 0.06$), and H_2O has a minor contribution to the separation of charges ($\delta = 0.00$–0.03). It is interesting to note that the charge distribution on the water decreases upon addition of NH_3 to the 2MSA–2MA–2H_2O complex.

Table 2 Dissociation energies with zero-point energy correction (D_e) and Gibbs free energies at 298 K (ΔG) at the level of B3LYP-D3/aug-cc-pVDZ. A positive value corresponds to an endothermic process. B represents the alkyl amines. B = base (MA or TMA)

	D_e (kcal mol^{-1})		ΔG (kcal mol^{-1})	
Dissociation reaction	MA	TMA	MA	TMA
MSA–B → MSA + B	15	20	4	9
MSA–B–NH_3 → MSA + B + NH_3	29	29	10	10
2MSA–2B → 2MSA + 2B	68	63	35	30
2MSA–2B–2NH_3 → 2MSA + 2B + 2NH_3	92	89	40	35
MSA–B–H_2O → MSA + B + H_2O	30	32	10	9
MSA–B–NH_3–H_2O → MSA + B + NH_3 + H_2O	43	40	15	11
2MSA–2B–2H_2O → 2MSA + 2B + 2H_2O	95	80	42	27
2MSA–2B–2H_2O–2NH_3 → 2MSA + 2B + 2H_2O + 2NH_3	112	113	42	41

(B) MSA + TMA ($\pm NH_3$) system

(1) Dry conditions. Fig. 5a presents N_{total} values for the MSA + TMA reaction system ([MSA] = 7.9×10^{10} molecules per cm^3; [TMA] = 5.0×10^{10} molecules per cm^3), in the presence or absence of NH_3, as a function of reaction time. Under dry conditions, the MSA + TMA reaction is not very effective at forming particles, where only 2 particles cm^3 are detected at 5.9 s. However, as seen in Fig. 5a and b, adding NH_3 at about half the concentration of TMA ([NH_3] = 2.2×10^{10} molecules per cm^3) produced an immediate enhancement by four orders of magnitude in N_{total} (Table 1). Fig. 5c shows the corresponding size distributions when NH_3 is present (too few particles above 2.0 nm were generated in the MSA + TMA system alone to be measured by SMPS). In addition to the increase in the particle number concentration, the particles are observed to grow over time, with the GMD increasing from 4.0 ± 0.1 nm at 1.7 s to 5.4 ± 0.1 nm at 5.9 s (Fig. S9a†). The particle formation rate ($J_{>2.0nm}$) was estimated based on the SMPS data to be (7.6 ± 0.5) $\times 10^3$ particles per cm^3 per s under these conditions (Fig. S9b†).

A separate set of experiments was carried out at various concentrations of NH_3 (0 to 10×10^{10} molecules per cm^3) while keeping MSA and TMA constant ([MSA] = 6.4×10^{10} molecules per cm^3; [TMA] = 4.8×10^{10} molecules per cm^3). As seen in Fig. 6a, N_{total} increased with the concentration of NH_3. Enhancement factors were estimated from this dataset and are shown as a function of the NH_3 concentration in Fig. 6b. At NH_3 concentrations < 1.4×10^{10} molecules per cm^3 (0.55 ppb), some enhancement is already observed (EF < 100), but at [NH_3] > 1.9

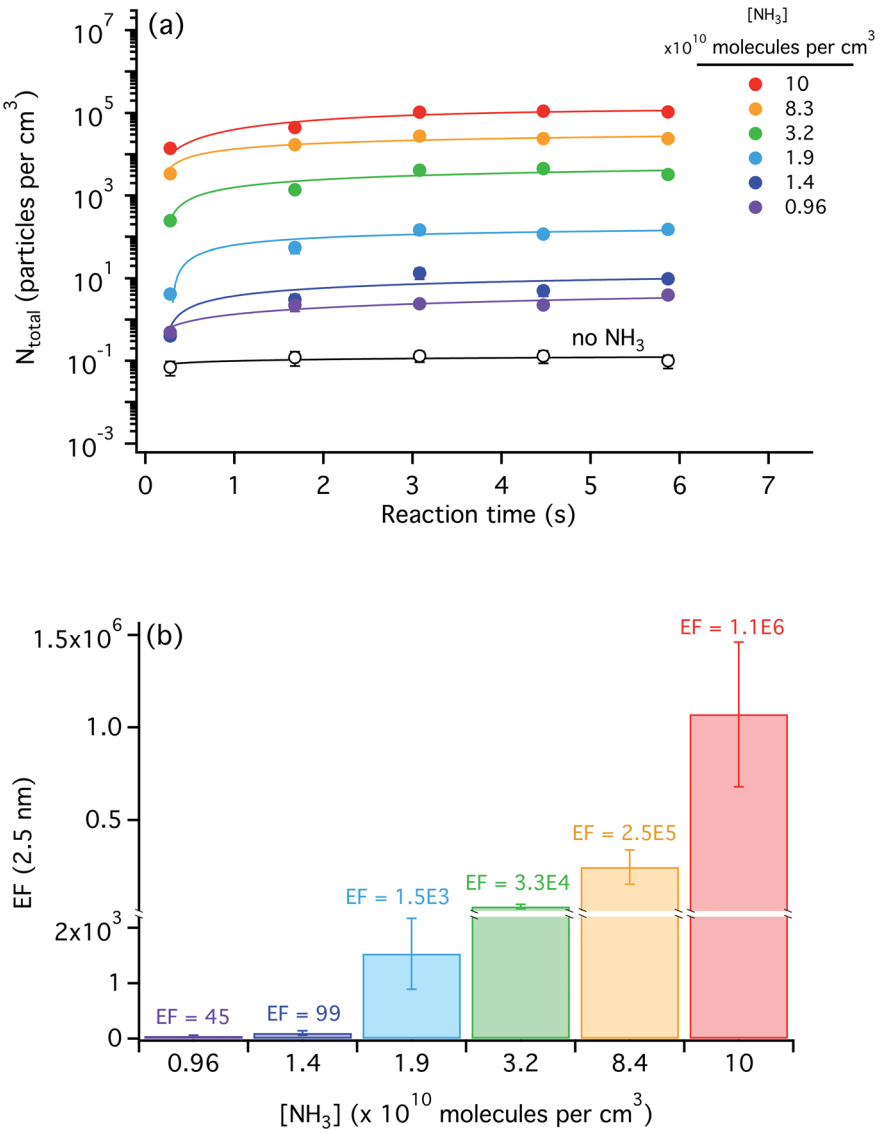

Fig. 6 (a) Total particle concentrations (N_{total}) from MSA + TMA + NH_3 reactions for varying NH_3 concentrations as a function of reaction time measured using the CPC (dry conditions; each point corresponds to an average from three replicate CPC measurements ± 1 standard deviation made over 2 min each). (b) Enhancement factor for particles measured as a function of NH_3 concentration (data for $t = 5.9$ s). Concentrations of reactants are [MSA] = 6.4×10^{10} molecules per cm^3; [TMA] = 4.8×10^{10} molecules per cm^3; [NH_3] = (0–10) $\times 10^{10}$ molecules per cm^3.

$\times 10^{10}$ molecules per cm^3 (> 0.78 ppb), the enhancement factor becomes 3 to 6 orders of magnitude, with EF reaching $\sim 10^6$ at $[NH_3] = 10 \times 10^{10}$ molecules per cm^3 (4.1 ppb). Thus, the presence of NH_3 even at relatively small concentrations drastically enhances NPF in the MSA + TMA system, which is not very efficient in forming particles on its own. Particle nucleation rates ($J_{>2.0nm}$) were estimated from the CPC data (no SMPS measurements were performed for this dataset) and ranged between 1.3 particles per cm^3 per s to 3.2×10^4 particles per cm^3 per s for NH_3 concentrations of $(0.96–10) \times 10^{10}$ particles per cm^3 (Fig. S10†). In short, although the MSA + TMA system is not very efficient at producing particles on its own, adding NH_3 can give particle nucleation rates similar to that of the MSA + MA system (Fig. S6b†).

The above MSA + TMA experiments were performed with excess MSA ([MSA]/[TMA] $\sim$ 1.6). Additional experiments were performed at various [MSA]/[TMA] ratios (Fig. S11†). In these, a large enhancement upon addition of NH_3 was systematically observed for each condition, and for an equal concentration of MSA and TMA ([MSA] = [TMA] = 6.4×10^{10} molecules per cm^3), the enhancement was still about 2 orders of magnitude under dry conditions. Note that the enhancement is not simply due to increase of condensing vapors. Indeed, as illustrated in Fig. S11,† for a fixed MSA concentration of 6.4×10^{10} molecules per cm^3 and an equivalent total base concentration, *i.e.* $\sim 3 \times 10^{10}$ molecules per cm^3, an enhancement is clearly visible when comparing to the MSA + TMA reaction alone (middle red bar; [total base] = [TMA] = 3×10^{10} molecules per cm^3; no NH_3). N_{total} observed at 5.3 s is 1.7 ± 0.3 particles per cm^3, whereas it is 216 ± 82 particles per cm^3 when NH_3 is present (keeping [total base] $\sim 3 \times 10^{10}$ molecules per cm^3; [TMA] = 1.4×10^{10} molecules per cm^3; [NH_3] = 1.8×10^{10} molecules per cm^3). For comparison, the total particle number concentration observed in the case of MSA + NH_3 alone ([NH_3] = [total base] = $(2.4–3.8) \times 10^{10}$ molecules per cm^3) is only 0.01–0.02 particles per cm^3 (Fig. S5†).

(2) In the presence of water vapor. Without NH_3 but in the presence of $\sim$45–50% RH (as seen from the comparison between the red trace in Fig. 5a and the orange trace in Fig. 7a), the addition of water to the MSA + TMA system ([MSA] = 7.9×10^{10} molecules per cm^3; [TMA] = 5.0×10^{10} molecules per cm^3) enhances new particle formation compared to the dry case (EF = $(1.8 \pm 0.4) \times 10^2$; Table 1). However, while N_{total} remains relatively small ($(4.1 \pm 0.1) \times 10^2$ molecules per cm^3 at 5.9 s), the particles are much larger, with a GMD of 20 ± 0.5 nm, compared to 4–5 nm for the dry case. This is also different from the MSA + MA reaction system where particles only grew to about 6 nm upon addition of water.

Upon addition of NH_3 (2.2×10^{10} molecules per cm^3) to the MSA + TMA + H_2O system, there is a clear enhancement in particle number concentration (Fig. 7a and b); however,

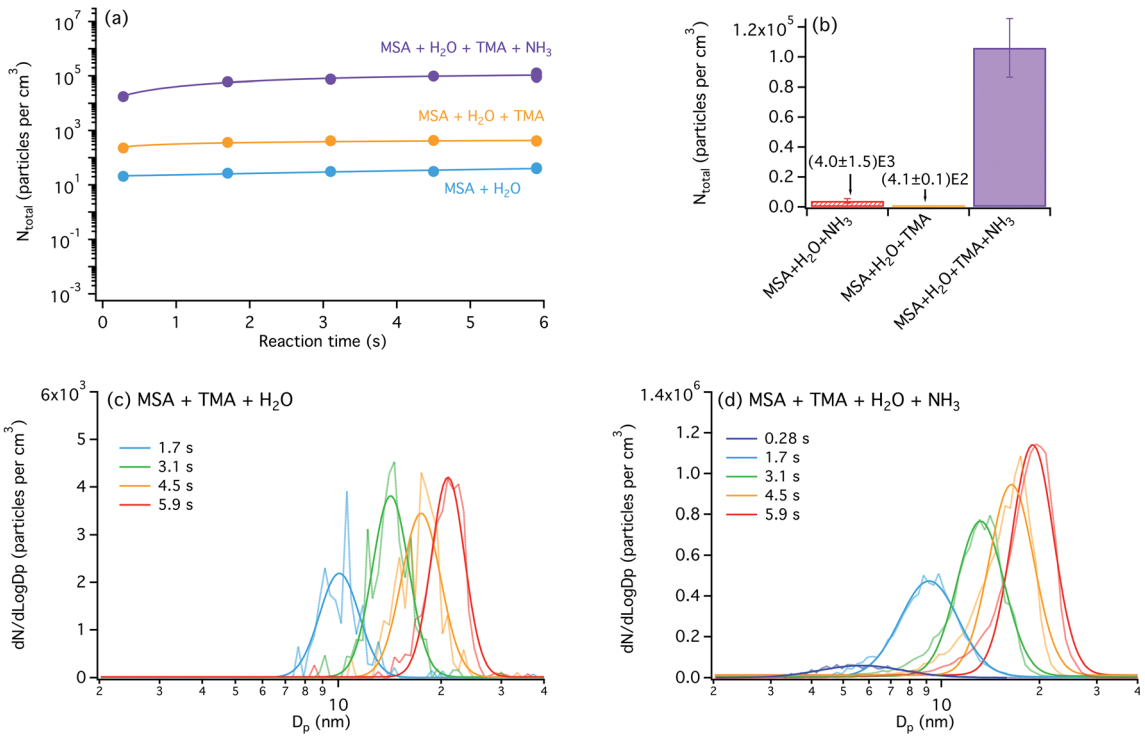

Fig. 7 (a) Total particle number concentrations (N_{total}) from MSA + TMA + H_2O and MSA + TMA + NH_3 + H_2O reactions as a function of reaction time measured using the CPC (RH $\sim$ 45–50%). Each data point corresponds to the average N_{total} measured over a 5 min scan (error bars correspond to 1 standard deviation). (b) Comparison of N_{total} values measured at 5.9 s for MSA + H_2O +NH_3, MSA + H_2O + TMA and MSA + H_2O + TMA + NH_3 reactions. Corresponding size distributions for (c) the MSA + TMA + H_2O reaction and (d) the MSA + TMA + H_2O + NH_3 reactions, respectively. Each size distribution is given in light colors with a log normal fit to guide the eye (each distribution corresponds to an average from five successive scans, except for reaction time 5.9 s where ten scans were averaged instead (standard deviation are not shown for clarity)). Concentrations of reactants for all panels are [MSA] = 7.9×10^{10} molecules per cm^3; [TMA] = 0 or 5.0×10^{10} molecules per cm^3; [NH_3] = 0 or 2.2×10^{10} molecules per cm^3.

as displayed in Table 1, the EF is less than that in the dry case ($EF = (2.6 \pm 0.5) \times 10^2$ under humid conditions, compared to 4 to 6 orders of magnitude under dry conditions). In this case, the particle mobility GMD for MSA + TMA is centered around 17.9 ± 0.4 nm, which is slightly smaller than that in the absence of NH_3. This suggests that while water is responsible for the

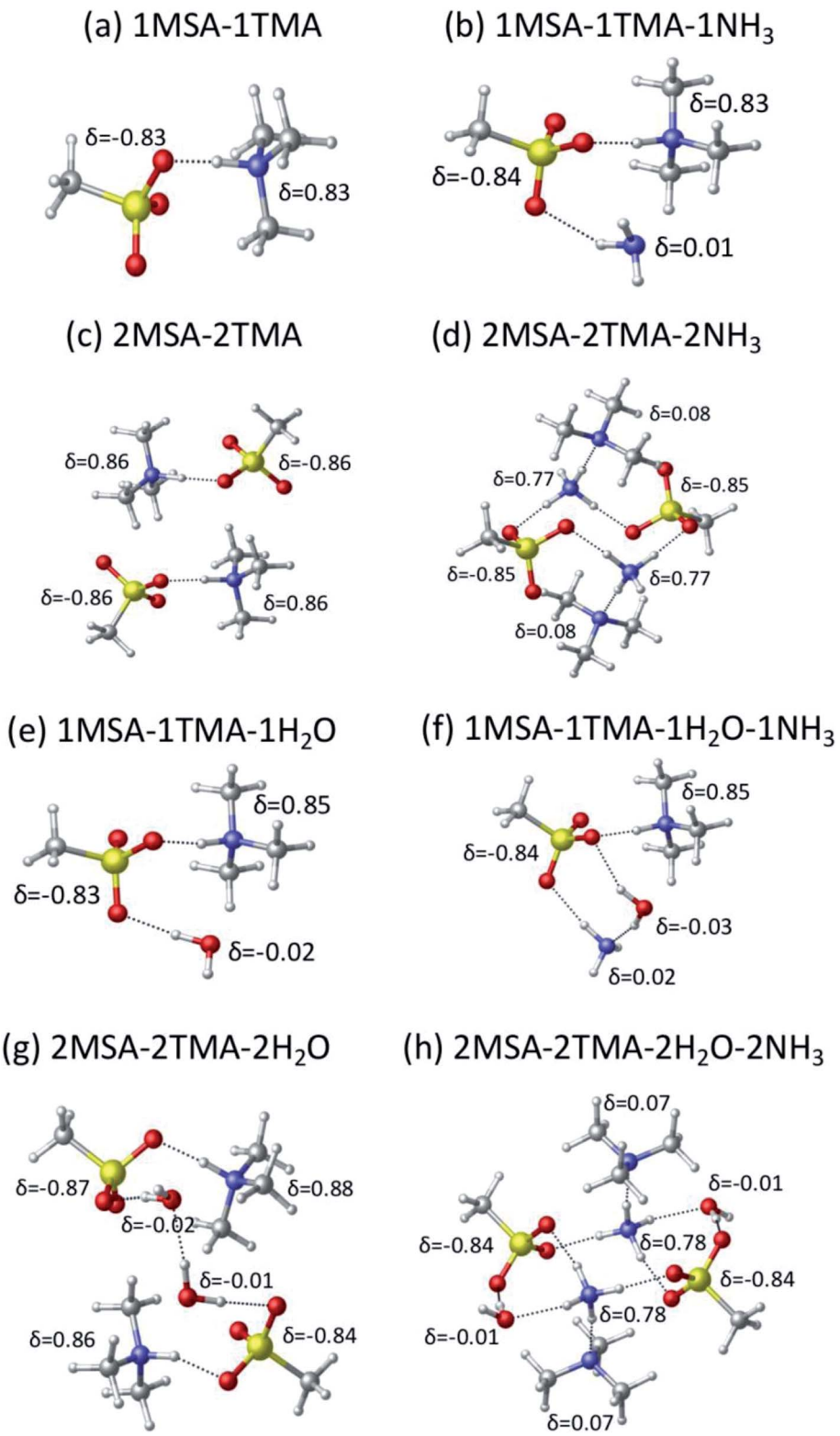

Fig. 8 Structures with distances (in angstroms) and partial charges δ (in atomic units) of the most stable structures of complexes composed of MSA, TMA, NH_3 and H_2O at the level of B3LYP-D3/aug-cc-pVDZ. Structures (a) and (c), (b) and (d), (e) and (g), (f) and (h) are the mono-cluster and dimer cluster of MSA–TMA, MSA–TMA–NH_3, MSA–TMA–H_2O, MSA–TMA–H_2O–NH_3 respectively.

growth of the particles, the main effect of NH_3 is to enhance nucleation to form new particles. Note that a lower, but still significant enhancement was observed for experiments performed under equivalent MSA and TMA conditions ([MSA] = [TMA] = 6.4×10^{10} molecules per cm^3; RH ~ 45–50%), with EF = 19 ± 11 in this case upon addition of NH_3 (1.8×10^{10} molecules per cm^3) (Fig. S12†).

From the size distributions measured for MSA + TMA + H_2O (Fig. 7c and d; [MSA] = 7.9×10^{10} molecules per cm^3; [TMA] = 5.0×10^{10} molecules per cm^3; RH ~ 45–50%), particle formation rates ($J_{>2.0nm}$) were determined (Fig. S13†) to be $(1.7 \pm 0.06) \times 10^2$ particles per cm^3 per s (no NH_3) and $(6.5 \pm 0.03) \times 10^4$ particles per cm^3 per s (with NH_3; [NH_3] = 2.2×10^{10} molecules per cm^3). The corresponding $J_{>2.0nm}$ value for MSA + TMA + NH_3 under dry conditions and equivalent concentrations of the reactants (Fig. S9†) was only 7.6×10^3 particles per cm^3 per s, suggesting that the presence of water greatly enhanced particle formation. In addition, the quaternary system MSA + TMA + H_2O + NH_3 appears to be as efficient at forming particles as the ternary MSA + MA + NH_3 reaction system (dry conditions; [MSA] = 6.4×10^{10} molecules per cm^3; [MA] = 6.1×10^{10} molecules per cm^3; [NH_3] = 2.9×10^{11} molecules per cm^3). However, the particles exhibit larger diameters (GMD = 17 nm for the quaternary MSA + TMA + H_2O + NH_3 system *versus* GMD ~ 3 nm for the ternary MSA + MA + NH_3 system).

(3) Insights from theoretical calculations. The structures of the most stable MSA–TMA clusters with and without NH_3 are presented in Fig. 8 and the corresponding dissociation energies and Gibbs free energies are in Table 2. In the case of the 1MSA–1TMA (Fig. 8a) and 2MSA–2TMA (Fig. 8c) clusters without NH_3, the most stable structures involve a proton transfer (δ = 0.83–0.86) between MSA and TMA forming an ion pair, consistent with our previous studies.[74,82,85] Note that for the 2MSA–2TMA cluster, there are no hydrogen bonds between the two MSA–TMA ion pairs, which is a distinct difference from the MSA–MA clusters presented above. The 2MSA–2TMA cluster is bound by Van der Waals interactions, of which the largest contribution is dipole–dipole interaction. Two dissociation pathways were considered for this cluster: 2MSA–2TMA ⇒ 2 MSA + 2 TMA and 2MSA–2TMA ⇒ 2 (MSA–TMA). The corresponding Gibbs free energies for the two pathways at T = 298 K are 30 kcal mol^{-1} and 12 kcal mol^{-1}, respectively. The free energy changes are positive in both indicating that the dissociation reactions are endothermic, and the cluster, if it is formed, is thermodynamically stable with respect to dissociation. However due to the absence of free –NH groups on TMA, the 2MSA–2TMA cluster does not have any potential hydrogen bonding opportunities for incoming molecules to attach to this cluster. This is consistent with the experimental observations that the MSA + TMA system is not very efficient at forming detectable particles.

The role of NH_3 in the 1MSA–1TMA–1NH_3 cluster (Fig. 8b) is similar to that observed in the MSA + MA system, where NH_3 simply attaches to the ion pair with minimal contribution to the separation of charges (δ = 0.01) and the proton transfer remains between MSA and TMA (δ = 0.83). However, for the 2MSA–2TMA–2NH_3 cluster (Fig. 8d), the structure surprisingly shows a significant change. In this case, the proton is transferred from MSA to NH_3 instead of to TMA. This is also seen in the partial charge distribution on NH_3 (δ = 0.77), showing that NH_3 now becomes the dominant acceptor. Similar observations were recently reported for H_2SO_4–dimethylamine–NH_3 clusters,[112] where NH_3 forms more intermolecular interactions than dimethylamine within the cluster and it was the species that accepts the proton from the acid, although dimethylamine is a stronger base (gas phase basicity,[175] GB = 896.5 kJ mol^{-1}).

When NH_3 is present, the 2MSA–2TMA–2NH_3 cluster (Fig. 8d) possesses a closed ring structure, where two NH_3 and two MSA form a core and TMA is bound on the outside of this core, unlike the 2MSA–2TMA open structure cluster (Fig. 8c). Although TMA is a much stronger base (gas phase basicity, GB = 918.1 kJ mol^{-1}),[175] NH_3 (GB = 819.0 kJ mol^{-1})[175] can form more hydrogen bonds, leading to a much more stable structure. Indeed, the dissociation energy increases from 63 to 89 kcal mol^{-1}, and the corresponding Gibbs free energy increases from 30 to 35 kcal mol^{-1} (Table 2). In addition, the presence of NH_4^+ in the cluster structure offers hydrogen bonding opportunities for incoming gases to potentially attach to the cluster and cause it to grow to detectable sizes. This remarkable shift in charge distribution, stability and structure of the clusters parallels the large enhancement observed in the experiments, where the presence of 1.0×10^{11} NH_3 molecules per cm^3 (Fig. 6) in the dry MSA + TMA reaction system induced enhancements in particle formation by up to six orders of magnitude.

Proton transfer occurs between MSA and TMA in the 1MSA–1TMA–1H_2O (Fig. 8e) and 2MSA–2TMA–2H_2O clusters (Fig. 8g), as well as for the 1MSA–1TMA–1H_2O–1NH_3 cluster (Fig. 8f). Note that, in the 2MSA–2TMA–2H_2O cluster (Fig. 8g), H_2O acts as a bridge between the ion pairs, increasing the stability of the cluster. In the 2MSA–2TMA–2NH_3–2H_2O cluster (Fig. 8h) involving NH_3, ammonia is the dominant proton acceptor (δ = 0.78) as observed in the dry system, and TMA and H_2O connect with the other species through hydrogen bonds. This is also consistent with the experiments, although a much smaller enhancement was observed in the presence of water vapor (~45–50% RH) compared to the dry case.

(C) Comparison of the addition of NH_3 *versus* the addition of H_2O

For the MSA + MA reaction system, which is already very efficient in forming small particles under dry conditions, the addition of NH_3 induces only a modest enhancement. However, water promotes growth, which enhances the concentrations of particles.

For the MSA + TMA system, a small amount of NH_3 is far more effective in enhancing new particle formation than the larger atmospherically relevant amounts of water. Indeed, the addition of NH_3 (2.2×10^{10} molecules per cm^3) to the MSA + TMA reaction system gave a large increase in particle formation of four orders of magnitude, compared to an increase of $(1.8 \pm 0.4) \times 10^2$ (Table 1) upon the addition of water at much higher concentrations, ~3×10^{17} molecules per cm^3 (equivalent to ~45–50% RH). The presence of NH_3 promotes the

formation of a strong hydrogen bonding network which enables the formation of stable clusters. In addition, NH_3 replaces the strong base TMA as the main proton acceptor in the dimer systems. On the other hand, water provides hydrogen bonding opportunities that help to grow the particles. This is seen in the much larger diameter observed upon the addition of water, compared to the respective dry cases (with and without NH_3).

It is important to note that the reverse addition (*i.e.* adding small amount of TMA to the binary MSA + NH_3 system) is also of atmospheric relevance. On its own, the binary dry system MSA + NH_3, even at high concentrations of NH_3 (up to 2.8×10^{11} molecules per cm^3), is not effective at forming particles (only ~5 particles per cm^3 observed at $t = 5.3$ s; Fig. S5;† [MSA] = 6.4×10^{10} molecules per cm^3). However, with both TMA (4.8×10^{10} molecules per cm^3) and NH_3 (1.0×10^{11} molecules per cm^3) present, N_{total} increased by $(2.1 \pm 0.5) \times 10^4$ (Fig. S14†).

(D) Atmospheric implications

In air, gas phase H_2SO_4 is generally recognized as the main driver for new particle formation. However, increasing numbers of laboratory studies[73,74,82–85] and field measurements[8,11,16,101,176–178] suggest that MSA may also contribute. For example, we determined in this study apparent particle formation rates that suggest that multicomponent systems involving MSA, amines and NH_3 may be very efficient at forming particles; however, direct application of these rates to atmospheric conditions is not straightforward. Nevertheless, evidence from field measurements show that MSA may be a key player in particle formation and growth. For example, MSA was measured in nucleation-mode particles above a forest canopy in Hyytiälä, Finland.[8,11] Recent measurements from the Arctic[176,177] indicated a strong correlation between summertime particle number concentrations and particulate MSA concentrations, a period during which sulfate content is lower. Furthermore, Kerminen *et al.*[101] showed that MSA was enhanced compared to nss-SO_4 in sub-100 nm particles collected in the Finnish Arctic.

In addition, the role of MSA in NPF is expected to increase in the future, as anthropogenic SO_2 declines worldwide.[86–91] In addition, polar sea-ice is melting at an increasing rate. This is altering the marine ecosystem, providing more open ocean surface, and as consequence, higher emissions of DMS (precursor to MSA). For example, Sharma *et al.*[179] reported higher MSA concentrations in particles as the seasonal ice cover was reduced throughout the Arctic region.

While there are not many simultaneous co-located measurements of MSA and amines, there is growing evidence that ambient particles containing MSA also contain significant amounts of aminium and/or aminium ions.[8,11,16,100,137–141] For example, Kollner *et al.*[139] reported the presence of trimethylamine, NH_3 and MSA in the same particles in the Canadian Arctic, while Muller *et al.*[141] reported the co-existence of MSA with MA and NH_3 (along with dimethylamine and diethylamine) from measurements performed in a marine environment at Cape Verde. In more polluted regions, such as agriculturally intensive areas where both ammonia and amines are present in relatively high concentrations,[115–117,131,180] the chemistry highlighted in the present study may also play a role. Thus, MSA and its precursor (DMS) have been previously measured in presence of amines and ammonia in agricultural settings.[88,181,182] For example, Feilberg *et al.*,[181] measured DMS and TMA from an experimental pig production farm in Denmark, and Sorooshian *et al.*[183] reported high concentrations of MSA in particles collected near a cattle feedlot in California (35 ng per m^3).

In short, MSA, amines and NH_3 co-exist in various environments in the atmosphere from remote to polluted locations. The results presented here suggest that when combined, those species may have a significant role in particle formation and growth, but clearly there is a need for more parallel measurements of those species as well as the composition of the smallest particles to fully assess the importance of this chemistry in air.

Conclusions

The present study demonstrates that ammonia systematically enhances particle formation from the reaction of MSA with MA and TMA to various degrees depending on the amine. For MSA + MA, the addition of $[NH_3] = 2.9 \times 10^{11}$ molecules per cm^3 gives only a small enhancement ($EF = 1.6 \pm 0.1$, dry conditions; little to no enhancement in the presence of water vapor). On the other hand, addition of much smaller NH_3 concentrations (2.2×10^{10} molecules per cm^3) to the MSA + TMA binary reaction system has a much larger impact, with EF up to 10^4 under dry conditions, but a smaller enhancement under humid conditions ($EF = (2.6 \pm 0.5) \times 10^2$). Most importantly, although NPF from the MSA + TMA system is not efficient on its own, upon addition of NH_3 this system becomes competitive with the highly effective MSA + MA system.

One of the highlights of this study is that for the MSA + TMA reaction system, the addition of only ppb levels of NH_3 produces a much larger impact on NPF than the addition of much higher concentrations of water (~45–50% RH corresponding to ~12 000 ppm). While NH_3 stabilizes the clusters by providing a network of hydrogen bonds, leading to stable detectable nuclei, water bridges ion pairs and provides hydrogen-bonding opportunities to grow the initial cluster to diameters of 17–20 nm. In the case of MSA + TMA, surprisingly, NH_3 even becomes the acceptor for the proton from MSA in larger clusters, despite its weaker gas phase basicity compared to TMA.

The powerful combination of experimental results and quantum chemical calculations highlights the molecular basis for synergy occurring in the acid–base reactions involving MSA with MA or TMA in the presence of NH_3. These results are of particular importance as NH_3 is ubiquitous in air, and is almost always simultaneously present with amines both outdoors and indoors.[115,132]

Conflicts of interest

There are no conflicts of interests to declare.

Acknowledgements

The authors are grateful to the National Science Foundation (Grants No. 1443140, 1337080 and 1928252) for supporting this research.

References

1 M. Kulmala and V. M. Kerminen, On the formation and growth of atmospheric nanoparticles, *Atmos. Res.*, 2008, **90**, 132–150.
2 M. Kulmala, H. Vehkamaki, T. Petaja, M. Dal Maso, A. Lauri, V. M. Kerminen, W. Birmili and P. H. McMurry, Formation and growth rates of ultrafine atmospheric particles: a review of observations, *J. Aerosol Sci.*, 2004, **35**, 143–176.
3 R. Y. Zhang, A. Khalizov, L. Wang, M. Hu and W. Xu, Nucleation and growth of nanoparticles in the atmosphere, *Chem. Rev.*, 2012, **112**, 1957–2011.
4 S. H. Lee, H. Gordon, H. Yu, K. Lehtipalo, R. Haley, Y. X. Li and R. Y. Zhang, New particle formation in the atmosphere: from molecular clusters to global climate, *J. Geophys. Res.: Atmos.*, 2019, **124**, 7098–7146.
5 C. O. Stanier, A. Y. Khlystov and S. N. Pandis, Nucleation events during the Pittsburgh air quality study: Description and relation to key meteorological, gas phase, and aerosol parameters, *Aerosol Sci. Technol.*, 2004, **38**, 253–264.
6 J. N. Smith, M. J. Dunn, T. M. VanReken, K. Iida, M. R. Stolzenburg, P. H. McMurry and L. G. Huey, Chemical composition of atmospheric nanoparticles formed from nucleation in Tecamac, Mexico: Evidence for an important role for organic species in nanoparticle growth, *Geophys. Res. Lett.*, 2008, **35**, 1–5.
7 H. Yu, A. G. Hallar, Y. You, A. Sedlacek, S. Springston, V. P. Kanawade, Y. N. Lee, J. Wang, C. G. Kuang, R. L. McGraw, I. McCubbin, J. Mikkila and S. H. Lee, Sub-3 nm particles observed at the coastal and continental sites in the United States, *J. Geophys. Res.: Atmos.*, 2014, **119**, 860–879.
8 J. M. Makela, S. Yli-Koivisto, V. Hiltunen, W. Seidl, E. Swietlicki, K. Teinila, M. Sillanpaa, I. K. Koponen, J. Paatero, K. Rosman and K. Hameri, Chemical composition of aerosol during particle formation events in boreal forest, *Tellus B*, 2001, **53**, 380–393.
9 P. Pillai, A. Khlystov, J. Walker and V. Aneja, Observation and analysis of particle nucleation at a forest site in Southeastern US, *Atmosphere*, 2013, **4**, 72–93.
10 K. Lehtipalo, M. Sipila, H. Junninen, M. Ehn, T. Berndt, M. K. Kajos, D. R. Worsnop, T. Petaja and M. Kulmala, Observations of nano-CN in the nocturnal boreal forest, *Aerosol Sci. Technol.*, 2011, **45**, 499–509.
11 M. J. Lawler, M. P. Rissanen, M. Ehn, R. L. Mauldin, N. Sarnela, M. Sipila and J. N. Smith, Evidence for diverse biogeochemical drivers of boreal forest new particle formation, *Geophys. Res. Lett.*, 2018, **45**, 2038–2046.
12 M. J. Lawler, J. Whitehead, C. O'Dowd, C. Monahan, G. McFiggans and J. N. Smith, Composition of 15-85 nm particles in marine air, *Atmos. Chem. Phys.*, 2014, **14**, 11557–11569.
13 R. J. Weber, P. H. McMurry, L. Mauldin, D. J. Tanner, F. L. Eisele, F. J. Brechtel, S. M. Kreidenweis, G. L. Kok, R. D. Schillawski and D. Baumgardner, A study of new particle formation and growth involving biogenic and trace gas species measured during ACE 1, *J. Geophys. Res.: Atmos.*, 1998, **103**, 16385–16396.
14 C. D. O'Dowd, M. Geever and M. K. Hill, New particle formation: Nucleation rates and spatial scales in the clean marine coastal environment, *Geophys. Res. Lett.*, 1998, **25**, 1661–1664.
15 D. B. Collins, J. Burkart, R. Y. W. Chang, M. Lizotte, A. Boivin-Rioux, M. Blais, E. L. Mungall, M. Boyer, V. E. Irish, G. Masse, D. Kunkel, J. E. Tremblay, T. Papakyriakou, A. K. Bertram, H. Bozem, M. Gosselin, M. Levasseur and J. P. D. Abbatt, Frequent ultrafine particle formation and growth in Canadian Arctic marine and coastal environments, *Atmos. Chem. Phys.*, 2017, **17**, 13119–13138.
16 M. Dall'Osto, D. C. S. Beddows, P. Tunved, R. Krejci, J. Strom, H. C. Hansson, Y. J. Yoon, K. T. Park, S. Becagli, R. Udisti, T. Onasch, C. D. O'Dowd, R. Simo and R. M. Harrison, Arctic sea ice melt leads to atmospheric new particle formation, *Sci. Rep.*, 2017, **7**, 1–10.
17 A. Singh, W. J. Bloss and F. D. Pope, 60 years of UK visibility measurements: Impact of meteorology and atmospheric pollutants on visibility, *Atmos. Chem. Phys.*, 2017, **17**, 2085–2101.
18 W. C. Hinds, *Aerosol Technology: Properties, Behavior, and Measurement of Airborne Particles*, John Wiley & sons Inc., New York, 1999.
19 D. Chang, Y. Song and B. Liu, Visibility trends in six megacities in China 1973-2007, *Atmos. Res.*, 2009, **94**, 161–167.
20 U. Pöschl, Atmospheric aerosols: Composition, transformation, climate and health effects, *Angew. Chem., Int. Ed.*, 2005, **44**, 7520–7540.
21 C. A. Pope and D. W. Dockery, Health effects of fine particulate air pollution: Lines that connect, *J. Air Waste Manage. Assoc.*, 2006, **56**, 709–742.
22 J. L. Mauderly and J. C. Chow, Health effects of organic aerosols, *Inhalation Toxicol.*, 2008, **20**, 257–288.
23 M. R. Heal, P. Kumar and R. M. Harrison, Particles, air quality, policy and health, *Chem. Soc. Rev.*, 2012, **41**, 6606–6630.
24 A. Nel, Air pollution-related illness: Effects of particles, *Science*, 2005, **308**, 804–806.
25 Intergovernmental Panel on Climate Change, *IPPC, Summary for Policymakers in: Climate Change 2013: The Physical Science Basis. Contribution of Working Group I to the Fifth Assessment Report of the Intergovernmental Panel on Climate Change*, Cambridge University Press, Cambridge, United Kingdom and New York, NY, USA, 2013.
26 M. Kanakidou, J. H. Seinfeld, S. N. Pandis, I. Barnes, F. J. Dentener, M. C. Facchini, R. Van Dingenen, B. Ervens, A. Nenes, C. J. Nielsen, E. Swietlicki,

J. P. Putaud, Y. Balkanski, S. Fuzzi, J. Horth, G. K. Moortgat, R. Winterhalter, C. E. L. Myhre, K. Tsigaridis, E. Vignati, E. G. Stephanou and J. Wilson, Organic aerosol and global climate modelling: A review, *Atmos. Chem. Phys.*, 2005, **5**, 1053–1123.

27 M. Hallquist, J. C. Wenger, U. Baltensperger, Y. Rudich, D. Simpson, M. Claeys, J. Dommen, N. M. Donahue, C. George, A. H. Goldstein, J. F. Hamilton, H. Herrmann, T. Hoffmann, Y. Iinuma, M. Jang, M. E. Jenkin, J. L. Jimenez, A. Kiendler-Scharr, W. Maenhaut, G. McFiggans, T. F. Mentel, A. Monod, A. S. H. Prevot, J. H. Seinfeld, J. D. Surratt, R. Szmigielski and J. Wildt, The formation, properties and impact of secondary organic aerosol: current and emerging issues, *Atmos. Chem. Phys.*, 2009, **9**, 5155–5236.

28 S. Fuzzi, U. Baltensperger, K. Carslaw, S. Decesari, H. D. van Der Gon, M. C. Facchini, D. Fowler, I. Koren, B. Langford, U. Lohmann, E. Nemitz, S. Pandis, I. Riipinen, Y. Rudich, M. Schaap, J. G. Slowik, D. V. Spracklen, E. Vignati, M. Wild, M. Williams and S. Gilardoni, Particulate matter, air quality and climate: Lessons learned and future needs, *Atmos. Chem. Phys.*, 2015, **15**, 8217–8299.

29 J. Almeida, S. Schobesberger, A. Kurten, I. K. Ortega, O. Kupiainen-Maatta, A. P. Praplan, A. Adamov, A. Amorim, F. Bianchi, M. Breitenlechner, A. David, J. Dommen, N. M. Donahue, A. Downard, E. Dunne, J. Duplissy, S. Ehrhart, R. C. Flagan, A. Franchin, R. Guida, J. Hakala, A. Hansel, M. Heinritzi, H. Henschel, T. Jokinen, H. Junninen, M. Kajos, J. Kangasluoma, H. Keskinen, A. Kupc, T. Kurten, A. N. Kvashin, A. Laaksonen, K. Lehtipalo, M. Leiminger, J. Leppa, V. Loukonen, V. Makhmutov, S. Mathot, M. J. McGrath, T. Nieminen, T. Olenius, A. Onnela, T. Petaja, F. Riccobono, I. Riipinen, M. Rissanen, L. Rondo, T. Ruuskanen, F. D. Santos, N. Sarnela, S. Schallhart, R. Schnitzhofer, J. H. Seinfeld, M. Simon, M. Sipila, Y. Stozhkov, F. Stratmann, A. Tome, J. Trostl, G. Tsagkogeorgas, P. Vaattovaara, Y. Viisanen, A. Virtanen, A. Vrtala, P. E. Wagner, E. Weingartner, H. Wex, C. Williamson, D. Wimmer, P. L. Ye, T. Yli-Juuti, K. S. Carslaw, M. Kulmala, J. Curtius, U. Baltensperger, D. R. Worsnop, H. Vehkamaki and J. Kirkby, Molecular understanding of sulphuric acid-amine particle nucleation in the atmosphere, *Nature*, 2013, **502**, 359–363.

30 T. Kurten, V. Loukonen, H. Vehkamaki and M. Kulmala, Amines are likely to enhance neutral and ion-induced sulfuric acid-water nucleation in the atmosphere more effectively than ammonia, *Atmos. Chem. Phys.*, 2008, **8**, 4095–4103.

31 H. Yu, R. McGraw and S. H. Lee, Effects of amines on formation of sub-3 nm particles and their subsequent growth, *Geophys. Res. Lett.*, 2012, **39**, 1–5.

32 W. A. Glasoe, K. Volz, B. Panta, N. Freshour, R. Bachman, D. R. Hanson, P. H. McMurry and C. Jen, Sulfuric acid nucleation: An experimental study of the effect of seven bases, *J. Geophys. Res.: Atmos.*, 2015, **120**, 1933–1950.

33 J. H. Zollner, W. A. Glasoe, B. Panta, K. K. Carlson, P. H. McMurry and D. R. Hanson, Sulfuric acid nucleation: power dependencies, variation with relative humidity, and effect of bases, *Atmos. Chem. Phys.*, 2012, **12**, 4399–4411.

34 J. Kirkby, J. Curtius, J. Almeida, E. Dunne, J. Duplissy, S. Ehrhart, A. Franchin, S. Gagne, L. Ickes, A. Kurten, A. Kupc, A. Metzger, F. Riccobono, L. Rondo, S. Schobesberger, G. Tsagkogeorgas, D. Wimmer, A. Amorim, F. Bianchi, M. Breitenlechner, A. David, J. Dommen, A. Downard, M. Ehn, R. C. Flagan, S. Haider, A. Hansel, D. Hauser, W. Jud, H. Junninen, F. Kreissl, A. Kvashin, A. Laaksonen, K. Lehtipalo, J. Lima, E. R. Lovejoy, V. Makhmutov, S. Mathot, J. Mikkila, P. Minginette, S. Mogo, T. Nieminen, A. Onnela, P. Pereira, T. Petaja, R. Schnitzhofer, J. H. Seinfeld, M. Sipila, Y. Stozhkov, F. Stratmann, A. Tome, J. Vanhanen, Y. Viisanen, A. Vrtala, P. E. Wagner, H. Walther, E. Weingartner, H. Wex, P. M. Winkler, K. S. Carslaw, D. R. Worsnop, U. Baltensperger and M. Kulmala, Role of sulphuric acid, ammonia and galactic cosmic rays in atmospheric aerosol nucleation, *Nature*, 2011, **476**, 429–433.

35 L. Yao, O. Garmash, F. Bianchi, J. Zheng, C. Yan, J. Kontkanen, H. Junninen, S. B. Mazon, M. Ehn, P. Paasonen, M. Sipila, M. Y. Wang, X. K. Wang, S. Xiao, H. F. Chen, Y. Q. Lu, B. W. Zhang, D. F. Wang, Q. Y. Fu, F. H. Geng, L. Li, H. L. Wang, L. P. Qiao, X. Yang, J. M. Chen, V. M. Kerminen, T. Petaja, D. R. Worsnop, M. Kulmala and L. Wang, Atmospheric new particle formation from sulfuric acid and amines in a Chinese megacity, *Science*, 2018, **361**, 278–281.

36 C. N. Jen, R. Bachman, J. Zhao, P. H. McMurry and D. R. Hanson, Diamine-sulfuric acid reactions are a potent source of new particle formation, *Geophys. Res. Lett.*, 2016, **43**, 867–873.

37 C. N. Jen, P. H. McMurry and D. R. Hanson, Stabilization of sulfuric acid dimers by ammonia, methylamine, dimethylamine, and trimethylamine, *J. Geophys. Res.: Atmos.*, 2014, **119**, 7502–7514.

38 J. Zhao, J. N. Smith, F. L. Eisele, M. Chen, C. Kuang and P. H. McMurry, Observation of neutral sulfuric acid-amine containing clusters in laboratory and ambient measurements, *Atmos. Chem. Phys.*, 2011, **11**, 10823–10836.

39 J. Elm, M. Passananti, T. Kurten and H. Vehkamaki, Diamines can initiate new particle formation in the atmosphere, *J. Phys. Chem. A*, 2017, **121**, 6155–6164.

40 H. B. Xie, J. Elm, R. Halonen, N. Myllys, T. Kurten, M. Kulmala and H. Vehkamaki, Atmospheric fate of monoethanolamine: enhancing new particle formation of sulfuric acid as an important removal process, *Environ. Sci. Technol.*, 2017, **51**, 8422–8431.

41 T. Berndt, F. Stratmann, M. Sipila, J. Vanhanen, T. Petaja, J. Mikkila, A. Gruner, G. Spindler, R. L. Mauldin, J. Curtius, M. Kulmala and J. Heintzenberg, Laboratory study on new particle formation from the reaction OH + SO_2: influence of experimental conditions, H_2O vapour,

NH_3 and the amine tert-butylamine on the overall process, *Atmos. Chem. Phys.*, 2010, **10**, 7101–7116.

42 T. Berndt, M. Sipila, F. Stratmann, T. Petaja, J. Vanhanen, J. Mikkila, J. Patokoski, R. Taipale, R. L. Mauldin and M. Kulmala, Enhancement of atmospheric H_2SO_4/H_2O nucleation: organic oxidation products *versus* amines, *Atmos. Chem. Phys.*, 2014, **14**, 751–764.

43 M. E. Erupe, A. A. Viggiano and S. H. Lee, The effect of trimethylamine on atmospheric nucleation involving H_2SO_4, *Atmos. Chem. Phys.*, 2011, **11**, 4767–4775.

44 T. Olenius, R. Halonen, T. Kurten, H. Henschel, O. Kupiainen-Maata, I. K. Ortega, C. N. Jen, H. Vehkamaki and I. Riipinen, New particle formation from sulfuric acid and amines: Comparison of monomethylamine, dimethylamine, and trimethylamine, *J. Geophys. Res.: Atmos.*, 2017, **122**, 7103–7118.

45 A. Kurten, F. Bianchi, J. Almeida, O. Kupiainen-Maatta, E. M. Dunne, J. Duplissy, C. Williamson, P. Barmet, M. Breitenlechner, J. Dommen, N. M. Donahue, R. C. Flagan, A. Franchin, H. Gordon, J. Hakala, A. Hansel, M. Heinritzi, L. Ickes, T. Jokinen, J. Kangasluoma, J. Kim, J. Kirkby, A. Kupc, K. Lehtipalo, M. Leiminger, V. Makhmutov, A. Onnela, I. K. Ortega, T. Petaja, A. P. Praplan, F. Riccobono, M. P. Rissanen, L. Rondo, R. Schnitzhofer, S. Schobesberger, J. N. Smith, G. Steiner, Y. Stozhkov, A. Tome, J. Trostl, G. Tsagkogeorgas, P. E. Wagner, D. Wimmer, P. L. Ye, U. Baltensperger, K. Carslaw, M. Kulmala and J. Curtius, Experimental particle formation rates spanning tropospheric sulfuric acid and ammonia abundances, ion production rates, and temperatures, *J. Geophys. Res.: Atmos.*, 2016, **121**, 12377–12400.

46 S. M. Ball, D. R. Hanson, F. L. Eisele and P. H. McMurry, Laboratory studies of particle nucleation: Initial results for H_2SO_4, H_2O, and NH_3 vapors, *J. Geophys. Res.: Atmos.*, 1999, **104**, 23709–23718.

47 D. R. Benson, M. E. Erupe and S. H. Lee, Laboratory-measured H_2SO_4-H_2O-NH_3 ternary homogeneous nucleation rates: initial observations, *Geophys. Res. Lett.*, 2009, **36**, 1–6.

48 K. Lehtipalo, L. Rondo, J. Kontkanen, S. Schobesberger, T. Jokinen, N. Sarnela, A. Kurten, S. Ehrhart, A. Franchin, T. Nieminen, F. Riccobono, M. Sipila, T. Yli-Juuti, J. Duplissy, A. Adamov, L. Ahlm, J. Almeida, A. Amorim, F. Bianchi, M. Breitenlechner, J. Dommen, A. J. Downard, E. M. Dunne, R. C. Flagan, R. Guida, J. Hakala, A. Hansel, W. Jud, J. Kangasluoma, V. M. Kerminen, H. Keskinen, J. Kim, J. Kirkby, A. Kupc, O. Kupiainen-Maatta, A. Laaksonen, M. J. Lawler, M. Leiminger, S. Mathot, T. Olenius, I. K. Ortega, A. Onnela, T. Petaja, A. Praplan, M. P. Rissanen, T. Ruuskanen, F. D. Santos, S. Schallhart, R. Schnitzhofer, M. Simon, J. N. Smith, J. Trostl, G. Tsagkogeorgas, A. Tome, P. Vaattovaara, H. Vehkamaki, A. E. Vrtala, P. E. Wagner, C. Williamson, D. Wimmer, P. M. Winkler, A. Virtanen, N. M. Donahue, K. S. Carslaw, U. Baltensperger, I. Riipinen, J. Curtius, D. R. Worsnop and M. Kulmala, The effect of acid-base clustering and ions on the growth of atmospheric nanoparticles, *Nat. Commun.*, 2016, **7**, 1–9.

49 M. Chen, M. Titcombe, J. K. Jiang, C. Jen, C. A. Kuang, M. L. Fischer, F. L. Eisele, J. I. Siepmann, D. R. Hanson, J. Zhao and P. H. McMurry, Acid-base chemical reaction model for nucleation rates in the polluted atmospheric boundary layer, *Proc. Natl. Acad. Sci. U. S. A.*, 2012, **109**, 18713–18718.

50 J. N. Smith, K. F. Moore, F. L. Eisele, D. Voisin, A. K. Ghimire, H. Sakurai and P. H. McMurry, Chemical composition of atmospheric nanoparticles during nucleation events in Atlanta, *J. Geophys. Res.: Atmos.*, 2005, **110**, 1–13.

51 A. Kurten, T. Jokinen, M. Simon, M. Sipila, N. Sarnela, H. Junninen, A. Adamov, J. Almeida, A. Amorim, F. Bianchi, M. Breitenlechner, J. Dommen, N. M. Donahue, J. Duplissy, S. Ehrhart, R. C. Flagan, A. Franchin, J. Hakala, A. Hansel, M. Heinritzi, M. Hutterli, J. Kangasluoma, J. Kirkby, A. Laaksonen, K. Lehtipalo, M. Leiminger, V. Makhmutov, S. Mathot, A. Onnela, T. Petaja, A. P. Praplan, F. Riccobono, M. P. Rissanen, L. Rondo, S. Schobesberger, J. H. Seinfeld, G. Steiner, A. Tome, J. Trostl, P. M. Winkler, C. Williamson, D. Wimmer, P. L. Ye, U. Baltensperger, K. S. Carslaw, M. Kulmala, D. R. Worsnop and J. Curtius, Neutral molecular cluster formation of sulfuric acid-dimethylamine observed in real time under atmospheric conditions, *Proc. Natl. Acad. Sci. U. S. A.*, 2014, **111**, 15019–15024.

52 F. Bianchi, A. P. Praplan, N. Sarnela, J. Dommen, A. Kurten, I. K. Ortega, S. Schobesberger, H. Junninen, M. Simon, J. Trostl, T. Jokinen, M. Sipila, A. Adamov, A. Amorim, J. Almeida, M. Breitenlechner, J. Duplissy, S. Ehrhart, R. C. Flagan, A. Franchin, J. Hakala, A. Hansel, M. Heinritzi, J. Kangasluoma, H. Keskinen, J. Kim, J. Kirkby, A. Laaksonen, M. J. Lawler, K. Lehtipalo, M. Leiminger, V. Makhmutov, S. Mathot, A. Onnela, T. Petaja, F. Riccobono, M. P. Rissanen, L. Rondo, A. Tome, A. Virtanen, Y. Viisanen, C. Williamson, D. Wimmer, P. M. Winkler, P. L. Ye, J. Curtius, M. Kulmala, D. R. Worsnop, N. M. Donahue and U. Baltensperger, Insight into acid-base nucleation experiments by comparison of the chemical composition of positive, negative, and neutral clusters, *Environ. Sci. Technol.*, 2014, **48**, 13675–13684.

53 S. Schobesberger, A. Franchin, F. Bianchi, L. Rondo, J. Duplissy, A. Kurten, I. K. Ortega, A. Metzger, R. Schnitzhofer, J. Almeida, A. Amorim, J. Dommen, E. M. Dunne, M. Ehn, S. Gagne, L. Ickes, H. Junninen, A. Hansel, V. M. Kerminen, J. Kirkby, A. Kupc, A. Laaksonen, K. Lehtipalo, S. Mathot, A. Onnela, T. Petaja, F. Riccobono, F. D. Santos, M. Sipila, A. Tome, G. Tsagkogeorgas, Y. Viisanen, P. E. Wagner, D. Wimmer, J. Curtius, N. M. Donahue, U. Baltensperger, M. Kulmala and D. R. Worsnop, On the composition of ammonia-sulfuric-acid ion clusters during aerosol particle formation, *Atmos. Chem. Phys.*, 2015, **15**, 55–78.

54 I. K. Ortega, O. Kupiainen, T. Kurten, T. Olenius, O. Wilkman, M. J. McGrath, V. Loukonen and H. Vehkamaki, From quantum chemical formation free energies to evaporation rates, *Atmos. Chem. Phys.*, 2012, **12**, 225–235.

55 V. Loukonen, T. Kurten, I. K. Ortega, H. Vehkamaki, A. A. H. Padua, K. Sellegri and M. Kulmala, Enhancing effect of dimethylamine in sulfuric acid nucleation in the presence of water - a computational study, *Atmos. Chem. Phys.*, 2010, **10**, 4961–4974.

56 J. W. DePalma, D. J. Doren and M. V. Johnston, Formation and growth of molecular clusters containing sulfuric acid, water, ammonia, and dimethylamine, *J. Phys. Chem. A*, 2014, **118**, 5464–5473.

57 L. J. Larson, A. Largent and F. M. Tao, Structure of the sulfuric acid-ammonia system and the effect of water molecules in the gas phase, *J. Phys. Chem. A*, 1999, **103**, 6786–6792.

58 H. Henschel, T. Kurten and H. Vehkamaki, Computational study on the effect of hydration on new particle formation in the sulfuric acid/ammonia and sulfuric acid/dimethylamine systems, *J. Phys. Chem. A*, 2016, **120**, 1886–1896.

59 J. N. Smith, K. C. Barsanti, H. R. Friedli, M. Ehn, M. Kulmala, D. R. Collins, J. H. Scheckman, B. J. Williams and P. H. McMurry, Observations of aminium salts in atmospheric nanoparticles and possible climatic implications, *Proc. Natl. Acad. Sci. U. S. A.*, 2010, **107**, 6634–6639.

60 B. R. Bzdek, M. J. Lawler, A. J. Horan, M. R. Pennington, J. W. DePalma, J. Zhao, J. N. Smith and M. V. Johnston, Molecular constraints on particle growth during new particle formation, *Geophys. Res. Lett.*, 2014, **41**, 6045–6054.

61 J. M. Creamean, A. P. Ault, J. E. Ten Hoeve, M. Z. Jacobson, G. C. Roberts and K. A. Prather, Measurements of aerosol chemistry during new particle formation events at a remote rural mountain site, *Environ. Sci. Technol.*, 2011, **45**, 8208–8216.

62 A. Kurten, A. Bergen, M. Heinritzi, M. Leiminger, V. Lorenz, F. Piel, M. Simon, R. Sitals, A. C. Wagner and J. Curtius, Observation of new particle formation and measurement of sulfuric acid, ammonia, amines and highly oxidized organic molecules at a rural site in central Germany, *Atmos. Chem. Phys.*, 2016, **16**, 12793–12813.

63 Q. Zhang, C. O. Stanier, M. R. Canagaratna, J. T. Jayne, D. R. Worsnop, S. N. Pandis and J. L. Jimenez, Insights into the chemistry of new particle formation and growth events in Pittsburgh based on aerosol mass spectrometry, *Environ. Sci. Technol.*, 2004, **38**, 4797–4809.

64 S. Schobesberger, H. Junninen, F. Bianchi, G. Lonn, M. Ehn, K. Lehtipalo, J. Dommen, S. Ehrhart, I. K. Ortega, A. Franchin, T. Nieminen, F. Riccobono, M. Hutterli, J. Duplissy, J. Almeida, A. Amorim, M. Breitenlechner, A. J. Downard, E. M. Dunne, R. C. Flagan, M. Kajos, H. Keskinen, J. Kirkby, A. Kupc, A. Kurten, T. Kurten, A. Laaksonen, S. Mathot, A. Onnela, A. P. Praplan, L. Rondo, F. D. Santos, S. Schallhart, R. Schnitzhofer, M. Sipila, A. Tome, G. Tsagkogeorgas, H. Vehkamaki, D. Wimmer, U. Baltensperger, K. S. Carslaw, J. Curtius, A. Hansel, T. Petaja, M. Kulmala, N. M. Donahue and D. R. Worsnop, Molecular understanding of atmospheric particle formation from sulfuric acid and large oxidized organic molecules, *Proc. Natl. Acad. Sci. U. S. A.*, 2013, **110**, 17223–17228.

65 M. R. Pennington, B. R. Bzdek, J. W. DePalma, J. N. Smith, A. M. Kortelainen, L. Hildebrandt Ruiz, T. Petaja, M. Kulmala, D. R. Worsnop and M. V. Johnston, Identification and quantification of particle growth channels during new particle formation, *Atmos. Chem. Phys.*, 2013, **13**, 10215–10225.

66 S. Chee, N. Myllys, K. C. Barsanti, B. M. Wong and J. N. Smith, An experimental and modeling study of nanoparticle formation and growth from dimethylamine and nitric acid, *J. Phys. Chem. A*, 2019, **123**, 5640–5648.

67 S. M. Murphy, A. Sorooshian, J. H. Kroll, N. L. Ng, P. Chhabra, C. Tong, J. D. Surratt, E. Knipping, R. C. Flagan and J. H. Seinfeld, Secondary aerosol formation from atmospheric reactions of aliphatic amines, *Atmos. Chem. Phys.*, 2007, **7**, 2313–2337.

68 I. Napari, M. Kulmala and H. Vehkamaki, Ternary nucleation of inorganic acids, ammonia, and water, *J. Chem. Phys.*, 2002, **117**, 8418–8425.

69 F. M. Tao, Gas phase proton transfer reaction of nitric acid ammonia and the role of water, *J. Chem. Phys.*, 1998, **108**, 193–202.

70 F. M. Tao, Direct formation of solid ammonium chloride particles from HCl and NH_3 vapors, *J. Chem. Phys.*, 1999, **110**, 11121–11124.

71 M. Luria and B. Cohen, Kinetics of gas to particle conversion in the NH_3-HCl system, *Atmos. Environ.*, 1980, **14**, 665–670.

72 J. Chen, S. Jiang, Y. R. Liu, T. Huang, C. Y. Wang, S. K. Miao, Z. Q. Wang, Y. Zhang and W. Huang, Interaction of oxalic acid with dimethylamine and its atmospheric implications, *RSC Adv.*, 2017, **7**, 6374–6388.

73 K. D. Arquero, R. B. Gerber and B. J. Finlayson-Pitts, The role of oxalic acid in new particle formation from methanesulfonic acid, methylamine, and water, *Environ. Sci. Technol.*, 2017, **51**, 2124–2130.

74 K. D. Arquero, J. Xu, R. B. Gerber and B. J. Finlayson-Pitts, Particle formation and growth from oxalic acid, methanesulfonic acid, trimethylamine and water: a combined experimental and theoretical study, *Phys. Chem. Chem. Phys.*, 2017, **19**, 28286–28301.

75 J. Zhao, A. Khalizov, R. Y. Zhang and R. McGraw, Hydrogen-bonding interaction in molecular complexes and clusters of aerosol nucleation precursors, *J. Phys. Chem. A*, 2009, **113**, 680–689.

76 W. Xu and R. Y. Zhang, A theoretical study of hydrated molecular clusters of amines and dicarboxylic acids, *J. Chem. Phys.*, 2013, **139**, 1–11.

77 K. H. Weber, Q. Liu and F. M. Tao, Theoretical study on stable small clusters of oxalic acid with ammonia and water, *J. Phys. Chem. A*, 2014, **118**, 1451–1468.

78 X. Q. Peng, T. Huang, S. K. Miao, J. Chen, H. Wen, Y. J. Feng, Y. Hong, C. Y. Wang and W. Huang, Hydration of oxalic acid-ammonia complex: atmospheric implication and Rayleigh-scattering properties, *RSC Adv.*, 2016, **6**, 46582–46593.

79 X. Q. Peng, Y. R. Liu, T. Huang, S. Jiang and W. Huang, Interaction of gas phase oxalic acid with ammonia and its atmospheric implications, *Phys. Chem. Chem. Phys.*, 2015, **17**, 9552–9563.

80 S. Patai and Z. Rappoport, *The Chemistry of sulphonic acids, esters and derivatives*, John Wiley & Sons Ltd, New York, 1991.

81 I. Barnes, J. Hjorth and N. Mihalopoulos, Dimethyl sulfide and dimethyl sulfoxide and their oxidation in the atmosphere, *Chem. Rev.*, 2006, **106**, 940–975.

82 M. L. Dawson, M. E. Varner, V. Perraud, M. J. Ezell, R. B. Gerber and B. J. Finlayson-Pitts, Simplified mechanism for new particle formation from methanesulfonic acid, amines, and water *via* experiments and *ab initio* calculations, *Proc. Natl. Acad. Sci. U. S. A.*, 2012, **109**, 18719–18724.

83 H. H. Chen, M. J. Ezell, K. D. Arquero, M. E. Varner, M. L. Dawson, R. B. Gerber and B. J. Finlayson-Pitts, New particle formation and growth from methanesulfonic acid, trimethylamine and water, *Phys. Chem. Chem. Phys.*, 2015, **17**, 13699–13709.

84 H. H. Chen and B. J. Finlayson-Pitts, New particle formation from methanesulfonic acid and amines/ammonia as a function of temperature, *Environ. Sci. Technol.*, 2017, **51**, 243–252.

85 H. H. Chen, M. E. Varner, R. B. Gerber and B. J. Finlayson-Pitts, Reactions of methanesulfonic acid with amines and ammonia as a source of new particles in air, *J. Phys. Chem. B*, 2016, **120**, 1526–1536.

86 Z. Klimont, S. J. Smith and J. Cofala, The last decade of global anthropogenic sulfur dioxide: 2000-2011 emissions, *Environ. Res. Lett.*, 2013, **8**, 1–6.

87 M. Amann, Z. Klimont and F. Wagner, Regional and global emissions of air pollutants: Recent trends and future scenarios, *Annu. Rev. Environ. Resour.*, 2013, **38**, 31–55.

88 V. Perraud, J. R. Horne, A. S. Martinez, J. Kalinowski, S. Meinardi, M. L. Dawson, L. M. Wingen, D. Dabdub, D. R. Blake, R. B. Gerber and B. J. Finlayson-Pitts, The future of airborne sulfur-containing particles in the absence of fossil fuel sulfur dioxide emissions, *Proc. Natl. Acad. Sci. U. S. A.*, 2015, **112**, 13514–13519.

89 J. G. Murphy, P. K. Gregoire, A. G. Tevlin, G. R. Wentworth, R. A. Ellis, M. Z. Markovic and T. C. VandenBoer, Observational constraints on particle acidity using measurements and modelling of particles and gases, *Faraday Discuss.*, 2017, **200**, 379–395.

90 D. I. Stern, Global sulfur emissions from 1850 to 2000, *Chemosphere*, 2005, **58**, 163–175.

91 U.S. EPA, https://www.epa.gov/air-trends/sulfur-dioxide-trends, accessed Sept. 16, 2019.

92 H. Berresheim, M. Adam, C. Monahan, C. O'Dowd, J. M. C. Plane, B. Bohn and F. Rohrer, Missing SO_2 oxidant in the coastal atmosphere? - Observations from high-resolution measurements of OH and atmospheric sulfur compounds, *Atmos. Chem. Phys.*, 2014, **14**, 12209–12223.

93 H. Berresheim, F. L. Eisele, D. J. Tanner, L. M. Mcinnes, D. C. Ramseybell and D. S. Covert, Atmospheric sulfur chemistry and cloud condensation nuclei (CCN) concentrations over the Northeastern Pacific Coast, *J. Geophys. Res.: Atmos.*, 1993, **98**, 12701–12711.

94 H. Berresheim, T. Elste, H. G. Tremmel, A. G. Allen, H. C. Hansson, K. Rosman, M. Dal Maso, J. M. Makela, M. Kulmala and C. D. O'Dowd, Gas-aerosol relationships of H_2SO_4, MSA, and OH: Observations in the coastal marine boundary layer at Mace Head, Ireland, *J. Geophys. Res.: Atmos.*, 2002, **107**, 1–12.

95 F. L. Eisele and D. J. Tanner, Measurement of the gas-phase concentration of H_2SO_4 and methane sulfonic-acid and estimates of H_2SO_4 production and loss in the atmosphere, *J. Geophys. Res.: Atmos.*, 1993, **98**, 9001–9010.

96 R. L. Mauldin, C. A. Cantrell, M. A. Zondlo, E. Kosciuch, B. A. Ridley, R. Weber and F. E. Eisele, Measurements of OH, H_2SO_4, and MSA during Tropospheric Ozone Production about the Spring Equinox (TOPSE), *J. Geophys. Res.: Atmos.*, 2003, **108**, 1–18.

97 R. L. Mauldin, D. J. Tanner, J. A. Heath, B. J. Huebert and F. L. Eisele, Observations of H_2SO_4 and MSA during PEM-Tropics-A, *J. Geophys. Res.: Atmos.*, 1999, **104**, 5801–5816.

98 H. Bardouki, H. Berresheim, M. Vrekoussis, J. Sciare, G. Kouvarakis, K. Oikonomou, J. Schneider and N. Mihalopoulos, Gaseous (DMS, MSA, SO_2, H_2SO_4 and DMSO) and particulate (sulfate and methanesulfonate) sulfur species over the northeastern coast of Crete, *Atmos. Chem. Phys.*, 2003, **3**, 1871–1886.

99 A. Jefferson, D. J. Tanner, F. L. Eisele, D. D. Davis, G. Chen, J. Crawford, J. W. Huey, A. L. Torres and H. Berresheim, OH photochemistry and methane sulfonic acid formation in the coastal Antarctic boundary layer, *J. Geophys. Res.: Atmos.*, 1998, **103**, 1647–1656.

100 M. C. Facchini, S. Decesari, M. Rinaldi, C. Carbone, E. Finessi, M. Mircea, S. Fuzzi, F. Moretti, E. Tagliavini, D. Ceburnis and C. D. O'Dowd, Important source of marine secondary organic aerosol from biogenic amines, *Environ. Sci. Technol.*, 2008, **42**, 9116–9121.

101 V. M. Kerminen, M. Aurela, R. E. Hillamo and A. Virkkula, Formation of particulate MSA: Deductions from size distribution measurements in the Finnish Arctic, *Tellus B*, 1997, **49**, 159–171.

102 L. N. Kolaitis, F. J. Bruynseels, R. E. Vangrieken and M. O. Andreae, Determination of methanesulfonic-acid and non-sea-salt sulfate in single marine aerosol-particles, *Environ. Sci. Technol.*, 1989, **23**, 236–240.

103 B. R. Bzdek, D. P. Ridge and M. V. Johnston, Reactivity of methanesulfonic acid salt clusters relevant to marine air, *J. Geophys. Res.: Atmos.*, 2011, **116**, D03301, DOI: 10.1029/2010jd015217.

104 B. R. Bzdek, D. P. Ridge and M. V. Johnston, Amine reactivity with charged sulfuric acid clusters, *Atmos. Chem. Phys.*, 2011, **11**, 8735–8743.
105 L. P. Chan and C. K. Chan, Displacement of ammonium from aerosol particles by uptake of triethylamine, *Aerosol Sci. Technol.*, 2012, **46**, 236–247.
106 C. Qiu, L. Wang, V. Lal, A. F. Khalizov and R. Y. Zhang, Heterogeneous reactions of alkylamines with ammonium sulfate and ammonium bisulfate, *Environ. Sci. Technol.*, 2011, **45**, 4748–4755.
107 N. Bork, J. Elm, T. Olenius and H. Vehkamaki, Methane sulfonic acid-enhanced formation of molecular clusters of sulfuric acid and dimethyl amine, *Atmos. Chem. Phys.*, 2014, **14**, 12023–12030.
108 H. J. Zhang, O. Kupiainen-Maatta, X. H. Zhang, V. Molinero, Y. H. Zhang and Z. S. Li, The enhancement mechanism of glycolic acid on the formation of atmospheric sulfuric acid-ammonia molecular clusters, *J. Chem. Phys.*, 2017, **146**, 1–11.
109 Y. Lin, Y. M. Ji, Y. X. Li, J. Secrest, W. Xu, F. Xu, Y. Wang, T. C. An and R. Y. Zhang, Interaction between succinic acid and sulfuric acid-base clusters, *Atmos. Chem. Phys.*, 2019, **19**, 8003–8019.
110 W. Xu and R. Y. Zhang, Theoretical investigation of interaction of dicarboxylic acids with common aerosol nucleation precursors, *J. Phys. Chem. A*, 2012, **116**, 4539–4550.
111 M. J. Lawler, P. M. Winkler, J. Kim, L. Ahlm, J. Trostl, A. P. Praplan, S. Schobesberger, A. Kurten, J. Kirkby, F. Bianchi, J. Duplissy, A. Hansel, T. Jokinen, H. Keskinen, K. Lehtipalo, M. Leiminger, T. Petaja, M. Rissanen, L. Rondo, M. Simon, M. Sipila, C. Williamson, D. Wimmer, I. Riipinen, A. Virtanen and J. N. Smith, Unexpectedly acidic nanoparticles formed in dimethylamine-ammonia-sulfuric-acid nucleation experiments at CLOUD, *Atmos. Chem. Phys.*, 2016, **16**, 13601–13618.
112 N. Myllys, S. Chee, T. Olenius, M. Lawler and J. N. Smith, Molecular-level understanding of synergistic effects in sulfuric acid-amine-ammonia mixed clusters, *J. Phys. Chem. A*, 2019, **123**, 2420–2425.
113 B. Temelso, E. F. Morrison, D. L. Speer, B. C. Cao, N. Appiah-Padi, G. Kim and G. C. Shields, Effect of mixing ammonia and alkylamines on sulfate aerosol formation, *J. Phys. Chem. A*, 2018, **122**, 1612–1622.
114 C. Y. Wang, S. Jiang, Y. R. Liu, H. Wen, Z. Q. Wang, Y. J. Han, T. Huang and W. Huang, Synergistic effect of ammonia and methylamine on nucleation in the Earth's atmosphere. A theoretical study, *J. Phys. Chem. A*, 2018, **122**, 3470–3479.
115 X. L. Ge, A. S. Wexler and S. L. Clegg, Atmospheric amines - Part I. A review, *Atmos. Environ.*, 2011, **45**, 524–546.
116 M. L. Dawson, V. Perraud, A. Gomez, K. D. Arquero, M. J. Ezell and B. J. Finlayson-Pitts, Measurement of gas-phase ammonia and amines in air by collection onto an ion exchange resin and analysis by ion chromatography, *Atmos. Meas. Tech.*, 2014, **7**, 2733–2744.
117 G. W. Schade and P. J. Crutzen, Emission of aliphatic-amines from animal husbandry and their reactions - Potential Source of N_2O and HCN, *J. Atmos. Chem.*, 1995, **22**, 319–346.
118 I. H. Chang, C. G. Lee and D. S. Lee, Development of an automated method for simultaneous determination of low molecular weight aliphatic amines and ammonia in ambient air by diffusion scrubber coupled to ion chromatography, *Anal. Chem.*, 2003, **75**, 6141–6146.
119 J. Xu, B. J. Finlayson-Pitts and R. B. Gerber, Proton transfer in mixed clusters of methanesulfonic acid, methylamine, and oxalic acid: implications for atmospheric particle formation, *J. Phys. Chem. A*, 2017, **121**, 2377–2385.
120 S. J. Li, L. L. Zhang, W. Qin and F. M. Tao, Intermolecular structure and properties of the methanesulfonic acid–ammonia system in small water clusters, *Chem. Phys. Lett.*, 2007, **447**, 33–38.
121 M. Kumar and J. S. Francisco, Ion pair particles at the air-water interface, *Proc. Natl. Acad. Sci. U. S. A.*, 2017, **114**, 12401–12406.
122 S. W. Gibb, R. F. C. Mantoura and P. S. Liss, Ocean-atmosphere exchange and atmospheric speciation of ammonia and methylamines in the region of the NW Arabian Sea, *Global Biogeochem. Cycles*, 1999, **13**, 161–177.
123 A. Vanneste, R. A. Duce and C. Lee, Methylamines in the marine atmosphere, *Geophys. Res. Lett.*, 1987, **14**, 711–714.
124 D. R. Hanson, P. H. McMurry, J. Jiang, D. Tanner and L. G. Huey, Ambient pressure proton transfer mass spectrometry: detection of amines and ammonia, *Environ. Sci. Technol.*, 2011, **45**, 8881–8888.
125 H. Yu and S. H. Lee, Chemical ionisation mass spectrometry for the measurement of atmospheric amines, *Environ. Chem.*, 2012, **9**, 190–201.
126 H. Hellen, A. J. Kieloaho and H. Hakola, Gas-phase alkyl amines in urban air; comparison with a boreal forest site and importance for local atmospheric chemistry, *Atmos. Environ.*, 2014, **94**, 192–197.
127 L. Yao, M. Y. Wang, X. K. Wang, Y. J. Liu, H. F. Chen, J. Zheng, W. Nie, A. J. Ding, F. H. Geng, D. F. Wang, J. M. Chen, D. R. Worsnop and L. Wang, Detection of atmospheric gaseous amines and amides by a high-resolution time-of-flight chemical ionization mass spectrometer with protonated ethanol reagent ions, *Atmos. Chem. Phys.*, 2016, **16**, 14527–14543.
128 T. C. VandenBoer, A. Petroff, M. Z. Markovic and J. G. Murphy, Size distribution of alkyl amines in continental particulate matter and their online detection in the gas and particle phase, *Atmos. Chem. Phys.*, 2011, **11**, 4319–4332.
129 T. C. VandenBoer, M. Z. Markovic, A. Petroff, M. F. Czar, N. Borduas and J. G. Murphy, Ion chromatographic separation and quantitation of alkyl methylamines and ethylamines in atmospheric gas and particulate matter using preconcentration and suppressed conductivity detection, *J. Chromatogr. A*, 2012, **1252**, 74–83.
130 N. A. Freshour, K. K. Carlson, Y. A. Melka, S. Hinz, B. Panta and D. R. Hanson, Amine permeation sources

characterized with acid neutralization and sensitivities of an amine mass spectrometer, *Atmos. Meas. Tech.*, 2014, **7**, 3611–3621.

131 J. Sintermann, S. Schallhart, M. Kajos, M. Jocher, A. Bracher, A. Munger, D. Johnson, A. Neftel and T. Ruuskanen, Trimethylamine emissions in animal husbandry, *Biogeosciences*, 2014, **11**, 5073–5085.

132 Y. You, V. P. Kanawade, J. A. de Gouw, A. B. Guenther, S. Madronich, M. R. Sierra-Hernandez, M. Lawler, J. N. Smith, S. Takahama, G. Ruggeri, A. Koss, K. Olson, K. Baumann, R. J. Weber, A. Nenes, H. Guo, E. S. Edgerton, L. Porcelli, W. H. Brune, A. H. Goldstein and S. H. Lee, Atmospheric amines and ammonia measured with a chemical ionization mass spectrometer (CIMS), *Atmos. Chem. Phys.*, 2014, **14**, 12181–12194.

133 J. M. Lobert, D. H. Scharffe, W. M. Hao and P. J. Crutzen, Importance of biomass burning in the atmospheric budgets of nitrogen-containing gases, *Nature*, 1990, **346**, 552–554.

134 K. Sellegri, M. Hanke, B. Umann, F. Arnold and M. Kulmala, Measurements of organic gases during aerosol formation events in the boreal forest atmosphere during QUEST, *Atmos. Chem. Phys.*, 2005, **5**, 373–384.

135 A. J. Kieloaho, H. Hellen, H. Hakola, H. E. Manninen, T. Nieminen, M. Kulmala and M. Pihlatie, Gas-phase alkylamines in a boreal Scots pine forest air, *Atmos. Environ.*, 2013, **80**, 369–377.

136 M. Hemmila, H. Hellen, A. Virkkula, U. Makkonen, A. P. Praplan, J. Kontkanen, L. Ahonen, M. Kulmala and H. Hakola, Amines in boreal forest air at SMEAR II station in Finland, *Atmos. Chem. Phys.*, 2018, **18**, 6367–6380.

137 A. Sorooshian, L. T. Padro, A. Nenes, G. Feingold, A. McComiskey, S. P. Hersey, H. Gates, H. H. Jonsson, S. D. Miller, G. L. Stephens, R. C. Flagan and J. H. Seinfeld, On the link between ocean biota emissions, aerosol, and maritime clouds: Airborne, ground, and satellite measurements off the coast of California, *Global Biogeochem. Cycles*, 2009, **23**, 1–15.

138 C. J. Gaston, K. A. Pratt, X. Y. Qin and K. A. Prather, Real-time detection and mixing state of methanesulfonate in single particles at an inland urban location during a phytoplankton bloom, *Environ. Sci. Technol.*, 2010, **44**, 1566–1572.

139 F. Kollner, J. Schneider, M. D. Willis, T. Klimach, F. Helleis, H. Bozem, D. Kunkel, P. Hoor, J. Burkart, W. R. Leaitch, A. A. Aliabadi, J. P. D. Abbatt, A. B. Herber and S. Borrmann, Particulate trimethylamine in the summertime Canadian high Arctic lower troposphere, *Atmos. Chem. Phys.*, 2017, **17**, 13747–13766.

140 M. D. Willis, J. Burkart, J. L. Thomas, F. Kollner, J. Schneider, H. Bozem, P. M. Hoor, A. A. Aliabadi, H. Schulz, A. B. Herber, W. R. Leaitch and J. P. D. Abbatt, Growth of nucleation mode particles in the summertime Arctic: a case study, *Atmos. Chem. Phys.*, 2016, **16**, 7663–7679.

141 C. Muller, Y. Iinuma, J. Karstensen, D. van Pinxteren, S. Lehmann, T. Gnauk and H. Herrmann, Seasonal variation of aliphatic amines in marine sub-micrometer particles at the Cape Verde islands, *Atmos. Chem. Phys.*, 2009, **9**, 9587–9597.

142 L. Ampollini, E. F. Katz, S. Bourne, Y. Tian, A. Novoselac, A. H. Goldstein, G. Lucic, M. S. Waring and P. F. DeCarlo, Observations and contributions of real-time indoor ammonia concentrations during HOMEChem, *Environ. Sci. Technol.*, 20019, **53**, 8591–8598.

143 F. M. Schmidt, O. Vaittinen, M. Metsala, M. Lehto, C. Forsblom, P. Groop and L. Halonen, Ammonia in breath and emitted from skin, *J. Breath Res.*, 2013, **7**, 1–14.

144 M. A. Sutton, U. Dragosits, Y. S. Tang and D. Fowler, Ammonia emissions from non-agricultural sources in the UK, *Atmos. Environ.*, 2000, **34**, 855–869.

145 H. H. Chen, M. J. Ezell, K. D. Arquero, M. E. Varner, M. L. Dawson, R. B. Gerber and B. J. Finlayson-Pitts, Correction: New particle formation and growth from methanesulfonic acid, trimethylamine and water, *Phys. Chem. Chem. Phys.*, 2017, **19**, 4893.

146 K. Neitola, D. Brus, U. Makkonen, M. Sipila, H. Lihavainen and M. Kulmala, Effect of addition of four base compounds on sulphuric-acid-water new-particle formation: a laboratory study, *Boreal Environ. Res.*, 2014, **19**, 257–274.

147 M. J. Ezell, H. Chen, K. D. Arquero and B. J. Finlayson-Pitts, Aerosol fast flow reactor for laboratory studies of new particle formation, *J. Aerosol Sci.*, 2014, **78**, 30–40.

148 J. Vanhanen, J. Mikkila, K. Lehtipalo, M. Sipila, H. E. Manninen, E. Siivola, T. Petaja and M. Kulmala, Particle size magnifier for nano-CN detection, *Aerosol Sci. Technol.*, 2011, **45**, 533–542.

149 J. Kangasluoma, H. Junninen, K. Lehtipalo, J. Mikkila, J. Vanhanen, M. Attoui, M. Sipila, D. Worsnop, M. Kulmala and T. Petaja, Remarks on ion generation for CPC detection efficiency studies in sub-3-nm size range, *Aerosol Sci. Technol.*, 2013, **47**, 556–563.

150 J. Kangasluoma, C. Kuang, D. Wimmer, M. P. Rissanen, K. Lehtipalo, M. Ehn, D. R. Worsnop, J. Wang, M. Kulmala and T. Petaja, Sub-3 nm particle size and composition dependent response of a nano-CPC battery, *Atmos. Meas. Tech.*, 2014, **7**, 689–700.

151 D. Wimmer, K. Lehtipalo, A. Franchin, J. Kangasluoma, F. Kreissl, A. Kurten, A. Kupc, A. Metzger, J. Mikkila, T. Petaja, F. Riccobono, J. Vanhanen, M. Kulmala and J. Curtius, Performance of diethylene glycol-based particle counters in the sub-3 nm size range, *Atmos. Meas. Tech.*, 2013, **6**, 1793–1804.

152 M. Hermann, B. Wehner, O. Bischof, H. S. Han, T. Krinke, W. Liu, A. Zerrath and A. Wiedensohler, Particle counting efficiencies of new TSI condensation particle counters, *J. Aerosol Sci.*, 2007, **38**, 674–682.

153 A. Kupc, O. Bischof, T. Tritscher, M. Beeston, T. Krinke and P. E. Wagner, Laboratory characterization of a new nano-water-based CPC 3788 and performance comparison to an ultrafine butanol-based CPC 3776, *Aerosol Sci. Technol.*, 2013, **47**, 183–191.

154 J. Xu, V. Perraud, B. J. Finlayson-Pitts and R. B. Gerber, Uptake of water by an acid-base nanoparticle: theoretical

and experimental studies of the methanesulfonic acid–methylamine system, *Phys. Chem. Chem. Phys.*, 2018, **20**, 22249–22259.

155 M. L. Dawson, M. E. Varner, V. Perraud, M. J. Ezell, J. Wilson, A. Zelenyuk, R. B. Gerber and B. J. Finlayson-Pitts, Amine-amine exchange in aminium-methanesulfonate aerosols, *J. Phys. Chem. C*, 2014, **118**, 29431–29440.

156 J. Xu, B. J. Finlayson-Pitts and R. B. Gerber, Nanoparticles grown from methanesulfonic acid and methylamine: microscopic structures and formation mechanism, *Phys. Chem. Chem. Phys.*, 2017, **19**, 31949–31957.

157 E. Burrell, T. Kar and J. C. Hansen, Computational study of the thermodynamics of new particle formation initiated by complexes of H_2SO_4-H_2O-NH_x, CH_3SO_3H-H_2O-NH_x, and HO_2-H_2O-NH_x, *ACS Earth Space Chem.*, 2019, **3**, 1415–1425.

158 N. Myllys, T. Olenius, T. Kurten, H. Vehkamaki, I. Riipinen and J. Elm, Effect of bisulfate, ammonia, and ammonium on the clustering of organic acids and sulfuric acid, *J. Phys. Chem. A*, 2017, **121**, 4812–4824.

159 A. B. Nadykto, F. Q. Yu, M. V. Jakovleva, J. Herb and Y. S. Xu, Amines in the Earth's atmosphere: a density functional theory study of the thermochemistry of pre-nucleation clusters, *Entropy*, 2011, **13**, 554–569.

160 S. S. Lv, S. K. Miao, Y. Ma, M. M. Zhang, Y. Wen, C. Y. Wang, Y. P. Zhu and W. Huang, Properties and atmospheric implication of methylamine sulfuric acid-water clusters, *J. Phys. Chem. A*, 2015, **119**, 8657–8666.

161 A. D. Becke, Density-functional thermochemistry. 3. The role of exact exchange, *J. Chem. Phys.*, 1993, **98**, 5648–5652.

162 R. G. Parr, *Density-Functional Theory of Atoms and Molecules*, Oxford University Press, 1994.

163 J. P. Perdew, J. A. Chevary, S. H. Vosko, K. A. Jackson, M. R. Pederson, D. J. Singh and C. Fiolhais, Atoms, molecules, solids, and surfaces - Applications of the generalized gradient approximation for exchange and correlation, *Phys. Rev. B: Condens. Matter Mater. Phys.*, 1992, **46**, 6671–6687.

164 S. Grimme, J. Antony, S. Ehrlich and H. Krieg, A consistent and accurate *ab initio* parametrization of density functional dispersion correction (DFT-D) for the 94 elements H-Pu, *J. Chem. Phys.*, 2010, **132**, 154104, DOI: 10.1063/1.3382344.

165 T. Kurten, M. Noppel, H. Vehkamaki, M. Salonen and M. Kulmala, Quantum chemical studies of hydrate formation of H_2SO_4 and HSO_4^-, *Boreal Environ. Res.*, 2007, **12**, 431–453.

166 J. P. Devlin, J. Sadlej, M. Hollman and V. Buch, Solvation stages of HCl and HBr in crystalline phases with methanol and small ethers: Acid-ether cluster complexes in amorphous and crystal phases, *J. Phys. Chem. A*, 2004, **108**, 2030–2043.

167 S. S. Xantheas, Ab-initio studies of cyclic water clusters $(H_2O)_n$, $n = 1$–6 - III. Comparison of density-functional with MP2 results, *J. Chem. Phys.*, 1995, **102**, 4505–4517.

168 Y. Miller, G. M. Chaban, J. Zhou, K. R. Asmis, D. M. Neumark and R. B. Gerber, Vibrational spectroscopy of $(SO_4^{2-})\cdot(H_2O)_n$ clusters, $n = 1$–5: Harmonic and anharmonic calculations and experiment, *J. Chem. Phys.*, 2007, **127**, 094305, DOI: 10.1063/1.2764074.

169 G. R. Medders, V. Babin and F. Paesani, A critical assessment of two-body and three-body interactions in water, *J. Chem. Theory Comput.*, 2013, **9**, 1103–1114.

170 J. M. Martinez and L. Martinez, Packing optimization for automated generation of complex system's initial configurations for molecular dynamics and docking, *J. Comput. Chem.*, 2003, **24**, 819–825.

171 L. Martinez, R. Andrade, E. G. Birgin and J. M. Martinez, PACKMOL: A package for building initial configurations for molecular dynamics simulations, *J. Comput. Chem.*, 2009, **30**, 2157–2164.

172 J. P. Foster and F. Weinhold, Natural hybrid orbitals, *J. Am. Chem. Soc.*, 1980, **102**, 7211–7218.

173 A. E. Reed and F. Weinhold, Natural bond orbital analysis of near-Hartree–Fock water dimer, *J. Chem. Phys.*, 1983, **78**, 4066–4073.

174 Y. H. Shao, Z. T. Gan, E. Epifanovsky, A. T. B. Gilbert, M. Wormit, J. Kussmann, A. W. Lange, A. Behn, J. Deng, X. T. Feng, D. Ghosh, M. Goldey, P. R. Horn, L. D. Jacobson, I. Kaliman, R. Z. Khaliullin, T. Kus, A. Landau, J. Liu, E. I. Proynov, Y. M. Rhee, R. M. Richard, M. A. Rohrdanz, R. P. Steele, E. J. Sundstrom, H. L. Woodcock, P. M. Zimmerman, D. Zuev, B. Albrecht, E. Alguire, B. Austin, G. J. O. Beran, Y. A. Bernard, E. Berquist, K. Brandhorst, K. B. Bravaya, S. T. Brown, D. Casanova, C. M. Chang, Y. Q. Chen, S. H. Chien, K. D. Closser, D. L. Crittenden, M. Diedenhofen, R. A. DiStasio, H. Do, A. D. Dutoi, R. G. Edgar, S. Fatehi, L. Fusti-Molnar, A. Ghysels, A. Golubeva-Zadorozhnaya, J. Gomes, M. W. D. Hanson-Heine, P. H. P. Harbach, A. W. Hauser, E. G. Hohenstein, Z. C. Holden, T. C. Jagau, H. J. Ji, B. Kaduk, K. Khistyaev, J. Kim, J. Kim, R. A. King, P. Klunzinger, D. Kosenkov, T. Kowalczyk, C. M. Krauter, K. U. Lao, A. D. Laurent, K. V. Lawler, S. V. Levchenko, C. Y. Lin, F. Liu, E. Livshits, R. C. Lochan, A. Luenser, P. Manohar, S. F. Manzer, S. P. Mao, N. Mardirossian, A. V. Marenich, S. A. Maurer, N. J. Mayhall, E. Neuscamman, C. M. Oana, R. Olivares-Amaya, D. P. O'Neill, J. A. Parkhill, T. M. Perrine, R. Peverati, A. Prociuk, D. R. Rehn, E. Rosta, N. J. Russ, S. M. Sharada, S. Sharma, D. W. Small, A. Sodt, T. Stein, D. Stuck, Y. C. Su, A. J. W. Thom, T. Tsuchimochi, V. Vanovschi, L. Vogt, O. Vydrov, T. Wang, M. A. Watson, J. Wenzel, A. White, C. F. Williams, J. Yang, S. Yeganeh, S. R. Yost, Z. Q. You, I. Y. Zhang, X. Zhang, Y. Zhao, B. R. Brooks, G. K. L. Chan, D. M. Chipman, C. J. Cramer, W. A. Goddard, M. S. Gordon, W. J. Hehre, A. Klamt, H. F. Schaefer, M. W. Schmidt, C. D. Sherrill, D. G. Truhlar, A. Warshel, X. Xu, A. Aspuru-Guzik, R. Baer, A. T. Bell, N. A. Besley, J. D. Chai, A. Dreuw, B. D. Dunietz, T. R. Furlani, S. R. Gwaltney, C. P. Hsu, Y. S. Jung, J. Kong, D. S. Lambrecht, W. Z. Liang, C. Ochsenfeld, V. A. Rassolov, L. V. Slipchenko, J. E. Subotnik, T. Van Voorhis, J. M. Herbert, A. I. Krylov, P. M. W. Gill and M. Head-Gordon, Advances in

molecular quantum chemistry contained in the Q-Chem 4 program package, *Mol. Phys.*, 2015, **113**, 184–215.

175 E. P. L. Hunter and S. G. Lias, Evaluated gas phase basicities and proton affinities of molecules: An update, *J. Phys. Chem. Ref. Data*, 1998, **27**, 413–656.

176 W. R. Leaitch, S. Sharma, L. Huang, D. Toom-Sauntry, A. Chivulescu, A.-M. Macdonald, K. von Salzen, J. R. Pierce, A. K. Bertram, J. C. Schroder, N. C. Shantz, R. Y.-W. Chang and A.-L. Norman, Dimethyl sulfide control of the clean summertime Arctic aerosol and cloud, *Elementa*, 2013, **1**, 1–12.

177 P. K. Quinn, T. L. Miller, T. S. Bates, J. A. Ogren, E. Andrews and G. E. Shaw, A 3-year record of simultaneously measured aerosol chemical and optical properties at Barrow, Alaska, *J. Geophys. Res.: Atmos.*, 2002, **107**, 4130, DOI: 10.1029/2001jd001248.

178 J. Burkart, M. D. Willis, H. Bozem, J. L. Thomas, K. Law, P. Hoor, A. A. Aliabadi, F. Kollner, J. Schneiders, A. Herber, J. P. D. Abbatt and W. R. Leaitch, Summertime observations of elevated levels of ultrafine particles in the high Arctic marine boundary layer, *Atmos. Chem. Phys.*, 2017, **17**, 5515–5535.

179 S. Sharma, E. Chan, M. Ishizawa, D. Toom-Sauntry, S. L. Gong, S. M. Li, D. W. Tarasick, W. R. Leaitch, A. Norman, P. K. Quinn, T. S. Bates, M. Levasseur, L. A. Barrie and W. Maenhaut, Influence of transport and ocean ice extent on biogenic aerosol sulfur in the Arctic atmosphere, *J. Geophys. Res.: Atmos.*, 2012, **117**, D12209, DOI: 10.1029/2011jd017074.

180 S. Trabue, K. Scoggin, L. McConnell, R. Maghirang, E. Razote and J. Hatfield, Identifying and tracking key odorants from cattle feedlots, *Atmos. Environ.*, 2011, **45**, 4243–4251.

181 A. Feilberg, D. Z. Liu, A. P. S. Adamsen, M. J. Hansen and K. E. N. Jonassen, Odorant emissions from intensive pig production measured by online proton-transfer-reaction mass spectrometry, *Environ. Sci. Technol.*, 2010, **44**, 5894–5900.

182 J. Filipy, B. Rumburg, G. Mount, H. Westberg and B. Lamb, Identification and quantification of volatile organic compounds from a dairy, *Atmos. Environ.*, 2006, **40**, 1480–1494.

183 A. Sorooshian, E. Crosbie, L. C. Maudlin, J. S. Youn, Z. Wang, T. Shingler, A. M. Ortega, S. Hersey and R. K. Woods, Surface and airborne measurements of organosulfur and methanesulfonate over the western United States and coastal areas, *J. Geophys. Res.: Atmos.*, 2015, **120**, 8535–8548.

